JAERI-Data/Code
98-011

DEVELOPMENT OF A NEW SIMULATION CODE FOR EVALUATION OF CRITICALITY TRANSIENTS INVOLVING FISSILE SOLUTION BOILING

March 1998

Benan BASOGLU*, Toshihiro YAMAMOTO,
Hiroshi OKUNO and Yasushi NOMURA

日本原子力研究所
Japan Atomic Energy Research Institute

本レポートは，日本原子力研究所が不定期に公刊している研究報告書です。
入手の問合わせは，日本原子力研究所研究情報部研究情報課（〒319-1195　茨城県那珂郡東海村）あて，お申し越しください。なお，このほかに財団法人原子力弘済会資料センター（〒319-1195　茨城県那珂郡東海村日本原子力研究所内）で複写による実費頒布をおこなっております。

This report is issued irregularly.
Inquiries about availability of the reports should be addressed to Research Information Division, Department of Intellectual Resources, Japan Atomic Energy Research Institute, Tokai-mura, Naka-gun, Ibaraki-ken, 319-1195, Japan.

編集兼発行　日本原子力研究所
印　　刷　いばらき印刷㈱

JAERI-Data/Code 98-011

Development of a New Simulation Code for Evaluation of Criticality Transients Involving Fissile Solution Boiling

Benan BASOGLU*, Toshihiro YAMAMOTO, Hiroshi OKUNO and Yasushi NOMURA

Department of Fuel Cycle Safety Research
Nuclear Safety Research Center
Tokai Research Establishment
Japan Atomic Energy Research Institute
Tokai-mura, Naka-gun, Ibaraki-ken

(Received January 30, 1998)

In this work, we report on the development of a new computer code named TRACE for predicting the excursion characteristics of criticality excursions involving fissile solutions. TRACE employs point neutronics coupled with simple thermal-hydraulics. The temperature, the radiolytic gas effects, and the boiling phenomena are estimated using the transient heat conduction equation, a lumped-parameter energy model, and a simple boiling model, respectively. To evaluate the model, we compared our results with the results of CRAC experiments. The agreement in these comparisons is quite satisfactory.

Keywords: Criticality Accident, Fissile Solution, Point Kinetics, Thermal-Hydraulics, Radiolytic Gas, Boiling, CRAC Experiment

* STA research fellow

JAERI-Data/Code 98-011

核分裂性溶液の沸騰を含む臨界過渡事象評価のためのシミュレーションコードの開発

日本原子力研究所東海研究所安全性試験研究センター燃料サイクル安全工学部
Benan BASOGLU*・山本　俊弘・奥野　　浩・野村　　靖

(1998年1月30日受理)

核分裂性溶液の臨界時の暴走特性を予測するための新しい計算コードＴＲＡＣＥの開発について報告する。ＴＲＡＣＥは簡易な熱水力と一点炉近似とを組み合わせたモデルを採用している。温度、放射線分解ガス効果、沸騰現象は、それぞれ時間依存の熱伝導方程式、lumped-parameterエネルギーモデルおよび簡易沸騰モデルを用いて算定される。これらのモデルの評価を、計算結果とＣＲＡＣ実験の結果とを比較することで行った。両者の一致は充分満足のいくものであった。

東海研究所：〒319－1195　茨城県那珂郡東海村白方白根２－４
＊ STAリサーチフェロー

Contents

目　　次

This is a blank page.

1. INTRODUCTION

Nuclear Criticality Safety plays an important role for fuel reprocessing plants since fuel reprocessing involves utilization of uranyl nitrate and plutonium nitrate solutions. In several known occasions, the power level of aqueous fissile solution systems became uncontrollable because of unexpected changes in system reactivity. Most of the industrial criticality accidents involved solution systems[1]. The consequences of these accidents were few fatalities and several significant overexposures to radiation. The largest total fission yield has been $4.x10^{19}$ fissions. Hence, there exists a need to investigate the consequences of accidental assembly of supercritical masses for aqueous fissile solutions.

The evaluation of on-site and off-site effects of criticality accidents requires an understanding of the potential consequences of such accidents. For any proposed accident, the first fission pulse may be considered as the most significant quantity. The first fission pulse determines the immediate consequences of the accident such as explosive destruction and dose rates to personnel before emergency evacuation. There is no actions that an individual can take to limit the consequences of the first pulse. Also, total fission yield determines the long-term dose at the plant boundary in continuing type accidents. A considerable amount of experimental and theoretical work has been conducted in the area of criticality safety to estimate first fission pulse and total fission yield of such excursions.

A good example is the KEWB* experiments which were conducted in the early 1960s[2]. In KEWB experiments, spherical and cylindrical vessels were used to determine safety characteristics of small aqueous reactors known as Water Boilers. The fuel for all experiments was 93% enriched $\mathbf{UO_2SO_4}$ (uranium sulfate) solution at uranium concentrations from 57 to 203 grams of ^{235}U per liter. A thick graphite reflector was used for both vessels, but some experiments were performed without the reflector on the cylindrical vessel. The excursions were initiated by poison rod withdrawal. SHEBA experiments were performed at the Los Alamos National Laboratory (LANL) using 5% enriched $\mathbf{UO_2F_2}$ (uranyl fluoride) solution to define the pulse characteristics of a low power

* KEWB stands for Kinetic Experiments on Water Boilers.

criticality in a solution[3]. SHEBA work also included a qualitative comparison of LOPCA (Low Power Criticality Accident) and SPIKE accidents.

Other examples of criticality experiments with fissile solutions include CRAC and SILENE. In late 1960s and early 1970s, CRAC experiments were performed by Commissariat à l'Énergie Atomique (CEA) at the Valduc facility using highly enriched $UO_2(NO_3)_2$ (uranyl nitrate) solution[4]. During these experiments, excursions were observed for a wide range of ramp reactivity additions and solution concentrations varying from 19.9 to 298 grams of ^{235}U per liter. SILENE is a homogeneous solution reactor fueled with 93% enriched $UO_2(NO_3)_2$ solution[5], and was also located at CEA Valduc facility. The core tank is a small annular tank where the excursions are initiated by a vertical rod. More than one thousand experiments have been conducted using the SILENE facility to study the first peak characteristics and integrated fission yields of solution criticality excursions. The results were useful to assess radiolytic gas release rates, boiling phenomena, and the pressure pulse wave associated with radiolytic gas formation due to the first fission pulse.

On 20th December, 1995, TRACY experimental facility has achieved its first criticality in Japan Atomic Energy Research Institute's research laboratories[6]. The TRACY core tank has an annular shape with 7.6 and 50 cm inner and outer diameters, respectively. The reactivity can be initiated by continuous feed of fuel solution into the core tank or by withdrawal of the transient rod. The TRACY experiments are intended to study several types of criticality excursions which may happen in a reprocessing plants.

Theoretical work resulted in development of several computer codes to predict fission rate and total fission yield for solution systems. One such analysis was conducted by David L. Hetrick of the University of Arizona[7]. He developed a one-region lumped-parameter model using the information obtained from experimental solution assemblies and from past criticality accidents. The model consists of an equation of state for water and radiolytic gas bubble mixture coupled with fluid acceleration and neutron dynamics. AIREK code was developed to predict the power bursts produced in KEWB experiments[2]. The AIREK can apply to a wide range of aqueous homogeneous fuel concentrations and

solution volumes contained in a vessel with an open free surface area. The void model for the AIREK code is restricted to step reactivity additions.

CRITEX code was developed by United Kingdom Atomic Energy Authority (UKAEA) to simulate the physical behavior for excursions in fissile solutions[8]. CRITEX code considers thermal-hydraulics in detail up to the point where boiling begins. CRITEX model includes radiolytic gas related events such as radiolytic gas generation, initial gas expansion, and bubble movement. CREST code was developed by Mitsubishi Atomic Power Industries Inc.-Japan for the analysis of power excursions involving fuel solutions[9]. The code solves the traditional point kinetics where the reactivity feedback is coupled with a single region thermal-hydraulics model. SKINATH-AR code was developed at the University of Tennessee to predict the results of hypothetical nuclear excursions involving an array of six polyethylene bottles containing an aqueous solution of low-enriched UO_2F_2 [10]. SKINATH-AR model employs point kinetics coupled with simple lumped parameter feedback for thermal and gas effects. Also, a simple quasi-steady-state model was developed by Dornier System GmbH-Germany for heating-up, nucleation and boiling of fissile solutions.

AGNES code was developed by Japan Atomic Energy Research Institute to investigate fuel criticality accidents in solution fuel systems[11), (12]. AGNES code utilizes two different void models for the radiolytic gas effects, namely the modified energy model and the pressure model. The modified energy model simulates power oscillations due to the void volume changes. The pressure model calculates the pressure pulse corresponding to the first fission pulse. More recently, CRITEX code was combined with CHAMPAGNE and DUV codes for a more detailed analysis[13]. The new code was named as CRITEX-CD. The new combined model considers the energy threshold at which radiolytic gas bubbles are released during criticality accidents. The initiation and growth of radiolytic gas bubbles are modeled using the CHAMPAGNE code. CRITEX-CD also calculates the hydrodynamic movement of the fissile liquid due to thermal expansion and bubble growth using the DUV code. The results of the experiments are frequently used to validate these computer codes.

In this work, we report on the development of a new simulation code for predicting excursion characteristics of fissile systems involving aqueous solution of uranium and plutonium. The new model uses point neutronics coupled with two-dimensional heat transfer model for predicting the temperature distribution, a new lumped-parameter energy model for calculating the radiolytic gas effects, and also a new boiling model for estimating the system power during boiling. Since, a very little computational work has been performed on excursion characteristics of boiling fissile solution systems, the emphasis is given for the accidents scenarios where the solution temperature reaches the boiling point. The results of this study will be useful in calculating the data required to understand the on-site and off-site effects of criticality accidents involving fissile solutions.

2. NEUTRONIC MODELING

2.1. Introduction

TRACE uses the traditional point kinetics equations to predict the time dependent total power history of the fissile solution systems. The point kinetics model assumes that the neutron flux is a product of a time-independent (steady-state) shape function and a time dependent amplitude function[14],[15]. The system is modeled as a point with no spatial effects. Therefore, these equations are an approximation in nature[16]. This section describes the neutronic modeling used in the TRACE code.

2.2. Point Neutronics

TRACE solves the following point neutronics equations:

$$\frac{d\mathbf{P}}{dt} = \left\{\frac{\rho_{total} - \beta}{\Lambda}\right\}\mathbf{P} + \sum_{i=1}^{m} \lambda_i C_i + S, \tag{2.1}$$

and

$$\frac{dC_i}{dt} = \frac{\beta_i}{\Lambda}\mathbf{P} - \lambda_i C_i \qquad i = 1,2,\ldots,m, \tag{2.2}$$

Here, β, Λ and ρ_{total} are interpreted as the total delayed neutron fraction, the neutron mean generation time (s), and the total system reactivity, respectively. Also, $\mathbf{P}$ is the total system power (J/s), C_i is the quantity proportional to the precursor concentration for group i (J/s), λ_i is the decay constant for precursor group i (s^{-1}), and S is the quantity proportional to the extraneous source neutron generation rate (J/s^2). The number of delayed neutron precursor groups, m, is equal to six for the presents analysis. Also, the total delayed neutron fraction β is equal to $\sum_i \beta_i$.

In the modeling described herein, it is assumed that point kinetics equations can provide a satisfactory estimate for the neutronic behavior of fissile liquid criticality transients. The initial values of the precursor concentrations are calculated such that they are in equilibrium with the initial power. The total fission yield, F, is calculated using the following differential equation:

$$\frac{dF}{dt} = \subset P. \tag{2.3}$$

Here $\subset$ is the conversion factor from Joule to fissions (fiss./J). TRACE assumes that calculations begin when the system attains delayed criticality ($k_{eff} = 1$) at time zero.

2.3. Reactivity Effects

The total system reactivity is composed of external and feedback reactivities:

$$\rho_{total} = \rho_{exter} + \rho_{fdbck}. \tag{2.4}$$

The external reactivity driving force function is the solution addition or the transient rod withdrawal. The solution addition provides a ramp reactivity input into the system. The transient rod withdrawal provides a ramp reactivity addition if the withdrawal speed is slow, a step reactivity addition if the withdrawal speed is fast.

For ramp reactivity addition, the estimation of external reactivity requires the calculation of the external reactivity driving force function with respect to solution height or with respect to the location of the transient rod in the system. This function is estimated by assuming that the external reactivity driving mechanism is separable from other reactivity mechanisms. To carry out the calculation of ρ_{exter} for solution feed ramp reactivity addition, the effective multiplication factor of the system is calculated using CSAS25 for different solution heights while keeping the density, temperature, and fuel concentration constant. CSAS25 is a control module of the SCALE system[17]. It activates the criticality safety analysis sequence which is designed to estimate the neutron multiplication factor for multi-dimensional systems. CSAS25 provides automated problem dependent cross-section processing followed by a effective multiplication factor calculation. It activates BONAMI and NITAWL to provide resonance corrected cross-sections based on the physical characteristics of the system being analyzed and KENO-V.a to calculate the effective multiplication factor. BONAMI performs Bondarenko calculations for resonance self-shielding for nuclides that have Bondarenko data associated with their cross-sections. Bondarenko treatment is typically used for unresolved range. NITAWL performs cross-section processing by applying the Nordheim resonance self-shielding correction to nuclides having resonance parameters. Nordheim integral treatment

is typically employed for resolved range. KENO-V.a is a three-dimensional multi-group Monte Carlo criticality program[18]. Also the 27 group cross-section library (27GROUPNDF4) is used for the calculations. This library contains 14 fast and 13 thermal groups and it has been extensively validated against critical systems involving plutonium and highly enriched uranium solutions.

The effective multiplication factor and the reactivity is related to each other as

$$\rho = \frac{k_{eff} - 1}{k_{eff}}. \tag{2.5}$$

A polynomial curve-fit to data points representing the reactivity with respect to the change in height may be used as the external reactivity driving force function. This function can be formulated as

$$\rho_{exter} = \mathcal{A}_1 (\Delta H) + \mathcal{A}_2 (\Delta H)^2 + \cdots + \mathcal{A}_n (\Delta H)^n. \tag{2.6}$$

Here, constants $\mathcal{A}_0$ to $\mathcal{A}_n$ are coefficients for the polynomial. The change in height can be calculated as

$$\Delta H = H - H_{crit}, \tag{2.7}$$

where H is the instantaneous height (m) and H_{crit} is the critical height (m). The quantities ΔH and ρ_{exter} are equal to zero at time zero.

TRACE can also employ an alternative approach to estimate the external reactivity. The following simple expression relates the external reactivity to the change in geometric buckling:

$$\rho_{exter} = \left(\frac{d\rho}{dB_g^2} \right) \Delta B_g^2. \tag{2.8}$$

For small reactivity changes, the derivative representing the change in reactivity with respect to change in geometric buckling may be approximated by the following linear relation:

$$\frac{d\rho}{dB_g^2} \approx \frac{\Delta\rho}{\Delta B_g^2} = \alpha_{B_g^2}, \tag{2.9}$$

where $\alpha_{B_g^2}$ is referred as the buckling reactivity coefficient. This coefficient may be calculated by fitting a functional line to the CSAS25 computed data representing the

reactivity with respect to the change in buckling. The slope of the line may be interpreted as the buckling reactivity coefficient. The geometric buckling for a finite cylinder based on one-group diffusion theory can be given by

$$B_g^2 = \left(\frac{\nu_0}{\tilde{R}}\right)^2 + \left(\frac{\pi}{\tilde{H}}\right)^2, \tag{2.10}$$

where $\tilde{R}$, $\tilde{H}$, and ν_0 are the extrapolated radius (m), the extrapolated height (m), and the smallest zero of Bessel function J_0 ($= 2.405$), respectively.* Using Equation (2.10) an expression for the change in buckling can be derived as

$$\Delta B_g^2 = \pi^2 \left\{ \frac{\left(\tilde{H}_{crit} - \tilde{H}\right)\left(\tilde{H}_{crit} + \tilde{H}\right)}{\tilde{H}^2 \tilde{H}_{crit}^2} \right\}, \tag{2.11}$$

where $\tilde{H}_{crit}$ is the extrapolated height of the critical system (m). Substituting Equation (2.9) and (2.11) into Equation (2.8) gives the following expression for the external reactivity in terms of the extrapolated height of the fissile liquid and the buckling reactivity coefficient:

$$\rho_{exter} = \alpha_{B_g^2} \pi^2 \left\{ \frac{\left(\tilde{H}_{crit} - \tilde{H}\right)\left(\tilde{H}_{crit} + \tilde{H}\right)}{\tilde{H}^2 \tilde{H}_{crit}^2} \right\}. \tag{2.12}$$

The reactivity feedback effects are quite important since they influence the amount of energy release. Previous set of experiments on fissile liquid transients (KEWB, CRAC, and SILENE) showed that main reactivity effects are attributed to the thermal expansion of solution due to temperature change, the formation of radiolytic gas voids, the change in fuel concentration, the fissile liquid motion, the formation of vapor bubbles due to boiling. The liquid height can also change due to the thermal expansion, the evolution of gas/vapor bubbles, and the surface evaporation.

For simplicity, the separability assumption is also utilized for the calculation of reactivity feedback functions. It is assumed that reactivity feedback mechanisms are truly separable from each other and feedback functions are calculated by treating each of the

* The extrapolated dimensions can be calculated as $\tilde{H} = H + 2\lambda_Z$ and $\tilde{R} = R + \lambda_R$. The quantities λ_Z and λ_R are the extrapolation lengths in axial and radial dimensions, respectively.

feedback effects separately.* The property whose feedback effect is under investigation is varied through a range while holding all other properties constant. This range is determined using the knowledge on the initial condition of the property and the expected minimum and maximum values that the property could attain during the transient. The effective multiplication factor, k_{eff}, of the system is calculated at several point in the range. With k_{eff} known, reactivity corresponding to a given state of the property can be calculated using Equation (2.5). The magnitude of the reactivity change is quantified as a function by fitting a polynomial to data points representing the reactivity with respect to the change in system property. The initial reactivity is assumed to zero for all feedback mechanisms.

For instance, to calculate the feedback reactivity due to temperature change, effective multiplication factor of the system is calculated using CSAS25 for different values of temperature by holding other thermodynamic and geometric quantities of the system constant. Then, system reactivity changes corresponding to temperature changes are estimated using Equation (2.5). A polynomial curve-fit to data points representing the reactivity with respect change in temperature is used as the temperature reactivity feedback function.

The reactivity feedback effect with respect to change in the void volume and the fuel concentration are calculated in a similar fashion by varying the volume fraction of the solution and the fuel concentration, respectively. TRACE can utilize power weighted and power-square weighted spatial reactivity weighting functions for temperature and void feedback effects. Reader should note that sudden introduction of large amount of void in the fissile liquid can change the neutron leakage and consequently the neutron flux significantly. In these instances, point kinetics model is invalid for predicting the system power.

Reactivity feedback effects of change in solution height due to the evaporation and the evolution of radiolytic gas/vapor bubbles are treated using the same function calculated for the external reactivity driving force. The estimation of reactivity feedback due to

* A weakness in using the separability approximation is the assumption of cross term feedback effects as being negligible.

motion is relatively complicated. The system volume can change significantly as a result of sudden increase in the pressure. Such a sudden change can introduce large perturbations in the fuel composition causing considerable deviations from the steady-state shape function assumption of the conventional point kinetics approach. In such circumstances, spatial dependence of the neutron flux has to be taken into account explicitly by using a quasistatic method. Nevertheless, in this work, the reactivity effect due to fluid motion is calculated using a simple approach by coupling the external reactivity driving force function and the void reactivity feedback function.

The separate feedback reactivity functions are then used to calculate the total feedback reactivity as

$$\rho_{fdbck} = \sum_{k} \rho_{fdbck,k} , \tag{2.13}$$

where $\rho_{fdbck,k}$ represent the change in reactivity for feedback effect k.

2.4. Initial Neutron Source Strength

Derivation of point kinetics equations assumes that the number of neutrons available in the system is large enough so that the statistical considerations are not important. If the criticality is established in the presence of weak neutron source, the early increase of power is stochastic in nature. The assembly can reach to a greater than critical mass before the first persistent chain reaction occur. The time location of the first persistent chain reaction and the actual amount of energy release can be much higher than that predicted by point kinetics equations. Hence, it is crucial to know the inherent neutron source strength for the neutronic analysis of criticality excursions.

Hansen identifies the following criteria for the "weak" neutron source[19]

$$\frac{2\mathcal{S}\tau}{\bar{\nu}\Gamma_2} << 1. \tag{2.14}$$

Here $\bar{\nu}$ is the average number of neutrons emitted per fission, τ is mean neutron lifetime (s), and $\mathcal{S}$ is the total neutron source strength (neutrons/s). The parameter Γ_2 is the Diven's factor which is formulated as $\overline{\nu(\nu-1)}/\bar{\nu}^2$. Equation (2.14) assumes that the

fissile system is near critical and $k_{eff} - 1$ is small such that $\lim_{k_{eff}-1\to 0}\left(k_{eff} - 1\right)/k_{eff} = k_{eff} - 1$ and the growth rate of neutron population is governed by an exponential behavior; $n_0 \exp\left\{\left[\left(k_{eff} - 1\right)/\tau\right]t\right\}$. This approximation is valid in the close vicinity of the prompt critical region. Table (2.1) provides the values of $\bar{\nu}$ and Γ_2 for selected fissionable isotopes.

Table 2.1

Mean Neutron Yield From Fission and Diven's Factor
For Selected Fissionable Isotopes[19]

Isotope	$\bar{\nu}$		Γ_2
	Thermal	Fast	(Diven's Parameter)
^{233}U	2.2366 ± 0.0069	2.62 ± 0.05	0.786 ± 0.013
^{235}U	2.4229 ± 0.0066	2.57 ± 0.04	0.795 ± 0.007
^{239}Pu	2.8799 ± 0.0090	3.09 ± 0.06	0.815 ± 0.017
^{241}Pu	2.934 ± 0.012	2.99 ± 0.06	0.807 ± 0.008

Therefore, estimation of the weak neutron source criteria requires the calculation of the total inherent neutron source strength. Uranyl nitrate solution contains primarily ^{234}U, ^{235}U, and ^{238}U isotopes of uranium and plutonium nitrate solution contains primarily ^{239}Pu and ^{240}Pu isotopes of plutonium[20]. All of these isotopes can disintegrate by spontaneous fission. Moreover, all nuclides of $A \geq 210$ and $Z > 83$ tend to decay by α-emission. In very heavy nuclides ($Z \geq 92$), decay by α-emission becomes very significant. The emitted α-particles have a very short range and they can react with light target atoms in the fissile liquid to generate neutrons[21]. Therefore, the total inherent neutron source strength can be written as

$$S = S^{SF} + S^{(\alpha,n)}, \tag{2.15}$$

where $\mathcal{S}^{SF}$ and $\mathcal{S}^{(\alpha,n)}$ are the inherent neutron source strength (neut./s) due to spontaneous fission and the (α,n)-reactions, respectively. The inherent neutron source strength from spontaneous fission may be calculated using

$$\mathcal{S}^{SF} = \left[\sum_j m_j Y_j^{SF}\right] V_{crit}, \tag{2.16}$$

Here, m_j is the specific weight of isotope j (kg/m^3), Y_j^{SF} is the rate of neutron production by spontaneous fission of isotope j (neut./s·kg), and V_{crit} is the critical volume (m^3). Likewise the number of neutrons produced by (α,n) reactions may be estimated using

$$\mathcal{S}^{(\alpha,n)} = \left[\sum_i \varepsilon_i \left(\sum_j m_j Y_{j,i}^{(\alpha,n)}\right)\right] V_{crit}, \tag{2.17}$$

where $Y_{j,i}^{(\alpha,n)}$ is the rate of neutron produced from the (α,n)-reactions between the α-particles released from isotope j and the target atoms of element i (neutrons/s·kg). The quantity ε_i in the Equation (2.17) can be calculated using

$$\varepsilon_i = \frac{f_i}{f_i + \sum_{k \neq i} f_k \mathcal{S}_{k/i}}, \tag{2.18}$$

where the $\mathcal{S}_{k/i}$ is the stopping power of element k relative to the element i. The quantities f_i and f_k is the atom number ratio of elements i and k, respectively.

For instance, the uranyl nitrate solution consists of hydrogen, nitrogen, oxygen, and uranium atoms. The isotopes ^{234}U, ^{235}U, and ^{238}U could emit α-particles and oxygen could react with these α-particles. Substituting Equations (2.16) and (2.17) into Equation (2.15) gives the following expression for the inherent neutron source strength of uranyl nitrate solution systems:

$$\mathcal{S} = \left[\sum_j m_j \left(Y_j^{SF} + \varepsilon_O Y_{j,O}^{(\alpha,n)}\right)\right] V_{crit}, \tag{2.19}$$

where

$$\varepsilon_O = \frac{f_O}{f_O + f_H \mathcal{S}_{H/O} + f_N \mathcal{S}_{N/O} + f_U \mathcal{S}_{U/O}}. \tag{2.20}$$

The quantities $S_{H/O}$, $S_{N/O}$, and $S_{U/O}$ are equal to 0.181, 0.915, and 4.803, respectively. Table 2.2 provides the values of Y_j^{SF} and $Y_{j,O}^{(\alpha,n)}$ for selected α-emitter isotopes. TRACE calculates the initial number densities (atoms/m^3) of the major elements that exist in the fissile liquid. It is assumed that the uranyl nitrate solution consists of four major components, namely, $UO_2(NO_3)_2$, H^+ (acid), free NO_3^-, and H_2O (water).* TRACE reads the uranium concentration, the weight percentage of uranium isotopes, the molarity of H^+, and the molarity of free NO_3^-. TRACE then computes the quantities $m_{^{234}U}$, $m_{^{235}U}$, and $m_{^{238}U}$ and the fractions f_H, f_O, f_N, and f_U. The inherent neutron source strength is estimated using Equations (2.19).

Preliminary studies using TRACE have shown that the inherent neutron source strength of uranyl nitrate solutions is generally very small. However, the inherent neutron source strength of plutonium nitrate is considerably higher than that of the uranyl nitrate, and statistical model may not be necessary for plutonium solutions.

Furthermore, Hawkins conducted experiments to investigate the neutron source of uranyl nitrate solutions[22]. The measurements were made with samples contained in one liter flasks. The fuel was 93% enriched in ^{235}U and the uranium content was 53 g/lt. The neutron production rate was reported to be equal to 5.6×10^3 neut./s·m^3.

* Similarly, plutonium nitrate solution consists of $Pu(NO_3)_4$, H^+ (acid), NO_3^- (base), and H_2O (water).

Table 2.2

Rate of Neutrons Produced by Spontaneous Fission and (α, n) Reactions with Oxygen Atoms Per Kg of the Isotope for Selected Isotopes[20].

Isotope j	Y_j^{ST} (neut./s·kg)	$Y_{j,O}^{(\alpha,n)}$ (neut./s·kg)
^{234}U	4.46×10^{0}	9.27×10^{3}
^{235}U	2.73×10^{-1}	2.14×10^{0}
^{238}U	1.08×10^{1}	2.34×10^{-1}
^{239}Pu	2.08×10^{1}	1.21×10^{5}
^{240}Pu	8.95×10^{5}	4.45×10^{5}

Seale and Anderson also investigated the neutron source strength in uranyl nitrate solutions[23]. The uranyl nitrate solution was 93% enriched in ^{235}U with an uranium content of 420 g/lt. A neutron production rate of 2.14×10^{4} neut./s·m^3 is reported for 25, 50, and 100 ml samples.*

Therefore, both calculational and experimental work have shown that the inherent neutron source strength from enriched uranyl nitrate solutions is small and the weak neutron source criteria shown in Equation (2.14) is satisfied. Consequently, the initial conditions should have spread of values and a statistical model is required for the evaluation of the time location and magnitude of the first persistent chain reaction. For ramp increase of reactivity, Hansen derives the probability of the first persistent chain reaction occurring at t_1 in a given time interval dt_1 as[19],[24]

$$P(t_1)dt_1 = \sqrt{\frac{2\dot{\alpha}\tau\varsigma^2}{\pi\bar{\nu}^2\Gamma_2^2}}\left[\frac{1-\mathrm{erf}\left(\sqrt{\frac{\dot{\alpha}}{2\tau}}t_1\right)}{2}\right]^{\left(\frac{2\varsigma\tau}{\bar{\nu}\Gamma_2}-1\right)}\exp\left(-\frac{\dot{\alpha}t_1^2}{2\tau}\right)dt_1. \quad (2.21)$$

* In the same study, the count rate increased 20 and 32 % for 500 and 1000 ml samples, respectively.

Here $\mathbf{erf}(x)$ is the error function* and $\dot{\alpha}$ is the ramp reactivity addition rate. Hansen also provides the following expression the average expected time elapsed between the system reaching a critical mass and the initiation of the first persistent chain:

$$\overline{t_1} = \sqrt{\frac{\pi \bar{\nu} \Gamma_2}{4 \dot{\alpha} S}}, \tag{2.22}$$

the standard deviation of the most likely location is given by Lutz as[25]

$$\sigma_1 = \sqrt{\left(1 - \frac{\pi}{4}\right) \frac{\bar{\nu} \Gamma_2}{\dot{\alpha} S}}. \tag{2.23}$$

According to Equation (2.22), the initiation time depends on the ramp reactivity addition rate and the inherent neutron source strength. The elapsed time between reaching a critical mass and the average time at which the first persistent chain reaction occur decreases as reactivity addition rate increases. Also as the inherent neutron source strength decreases, the expected initiation time increases

TRACE can consider the weak neutron source phenomenon by using a user-supplied initiation time. TRACE can start the criticality with a step input at the initiation time with a reactivity equal to the product of the ramp insertion rate of the reactivity and the initiation time of the first persistent chain as

$$\rho_{exter} = \begin{cases} 0 & if \quad t < t_{init} \\ \dot{\alpha} t_{init} & if \quad t = t_{init} \\ \dot{\alpha} t + \rho_{fdbck} & if \quad t > t_{init} \end{cases} \tag{2.24}$$

It is assumed that the most likely initiation time is given by Equation (2.22). Assuming a gaussian (normal) probability distribution, 10%, 50%, and 90% plausible initiation times are equal to $\overline{t_1} - 1.28\sigma_1$, $\overline{t_1}$, and $\overline{t_1} + 1.28\sigma_1$, respectively[16]. TRACE interprets these initiation times as

* Error function is given by

$$\mathbf{erf}(x) = \frac{2}{\sqrt{2}} \int_0^x \exp(-y^2) dy .$$

$$t_{init} = \begin{cases} \overline{t_1} - 1.28\sigma & \textit{for early initiation} \\ \overline{t_1} & \textit{for most likely initiation} \\ \overline{t_1} + 1.28\sigma & \textit{for late initiation} \end{cases} \tag{2.25}$$

3. THERMAL-HYDRAULIC MODELING

3.1. Introduction

Various models are incorporated in TRACE to describe thermal-hydraulic behavior of fissile liquids during criticality transients. TRACE assumes that the fissile liquid is contained in a cylindrical vessel which is open at the upper end. The temperature effects are estimated using two dimensional transient heat conduction equation. The system is divided into radial and axial regions and the time dependent temperature profiles are calculated for each region. The radiolytic gas effects are estimated using a lumped parameter model where it is assumed that the release of radiolytic gas is a threshold phenomenon. Following the attainment of the threshold, radiolytic gas bubbles nucleate, expand, and start moving upwards. TRACE also contains a new boiling model as an attempt to simulate a boiling system using appropriate correlations and equations. Moreover, a one-region pressure model is coupled with a simple equation of fluid motion to estimate acceleration of center of mass during fast transients. TRACE code does not consider radial distribution of radiolytic gas and vapor, at present. A description of thermal-hydraulic models used in TRACE is presented in this section.

3.2. Heat Transfer

The heat transfer model involves solution of the transient heat conduction equation in cylindrical coordinates. Assuming that the temperature is independent of the azimuthal angle, θ, the transient heat conduction equation for two-dimensional cylindrical geometry can be written as[26]

$$\frac{\partial T}{\partial t} = \alpha \left\{ \frac{\partial^2 T}{\partial r^2} + \frac{1}{r}\frac{\partial T}{\partial r} + \frac{\partial^2 T}{\partial z^2} + \frac{\Phi}{k} \right\}, \tag{3.1}$$

where α is equal to $k / \rho c_p$. Also, T is the temperature (K), k is the thermal conductivity (W/m·K), ρ is the density (kg/m^3), and c_p is the specific heat (J/kg·K). The power shape is represented by cosine and J_0 Bessel functions in axial and radial dimensions, respectively. The net rate of heat generation, Φ, is calculated from the energy

balance. The cylindrical system is divided into axial and radial regions where the space dependent terms in Equation (3.1) are expanded using finite differences[27]. Thus the partial differential equation reduces to a set of coupled ordinary differential equations which has time as the only independent variable. This coupled set of ordinary differential equations is used to estimate time dependent temperature profiles for axial and radial regions. The model also considers heat looses from bottom and side container walls. Heat loss from the container walls is by natural convection and radiation. For further discussions on natural convection and radiation equations and correlations used in this work, the reader is referred to Reference 16. The boundary condition on the axis of symmetry is taken to be

$$\lim_{r \to 0} \frac{1}{r} \frac{\partial T}{\partial r} = \frac{\partial^2 T}{\partial r^2} \quad . \tag{3.2}$$

In a liquid system, convection currents may arise due to the profile of the heat generation and such mixing could influence the temperature distribution of the system. This mixing phenomenon is also considered in our heat transfer model by using a mixing coefficient.

3.3. Radiolytic Gas

The power oscillations following the first fission pulse for the transient criticality of fissile liquids are attributed to the radiolytic gas phenomenon[24]. During criticality excursions, a large number of fission takes place. As the fission products are slowed down, the rapid transfer of energy to the medium along a track causes evaporation and radiolysis of the liquid into its constituents to form cylindrical microbubbles. Cylindrical shape is not stable and tend to form spherical microbubbles. These microbubbles consist of radiolytic gas and water vapor[28]. The atomic content of the radiolytic gas depends on the molecular structure of the fissile liquid. Radiolysis of water results in formation of free radicals*, positive ions, and molecular products[29],[30]. The free radicals present in water after the passage of radiation are $\bullet H$, e^-_{aq} (hydrated electron), $\bullet OH$, and $\bullet HO_2$ (hydroperoxy). All these radicals are highly reactive and they can react with the dissolved solutes in the

* Free radical is the reactive portion of a stable molecule occurring as a result of rupture of one or more single bonds by the ionizing radiation. All radicals are extremely reactive and have short life time.

solution. They can also recombine amongst themselves to form molecular products such as H_2, H_2O_2, H_2O, and O_2. The positive ion products of water radiolysis are H_2O^+, and to a less extent H_3O^+, H^+, and OH^+. The positive ions have short lives and they can recombine amongst themselves to yield free radicals. Also the molecular products of water radiolysis are H_2 and H_2O_2.

In low LET (Linear Energy Transfer) radiation such as electrons and γ-rays, ionization density is low and radicals can diffuse away from the local volume increasing the radical yields. In high LET radiation such as α-particles and fission fragments, radicals tend to combine and form the molecular products H_2 and H_2O_2 in the local volume due to high ionization density (cage effect). Consequently, radical yields are highest with low LET radiation while molecular product yields are highest with high LET radiation.

Bidwell, King, and Wykoff investigated the radiolytic yields of H_2 and N_2 gases based on the measurements from several water boiler uranyl nitrate solutions[31]. Average radiolytic yield of H_2 and N_2 was reported to be approximately equal to 7.4×10^{16} and 2.5×10^{14} molecules per joule of energy absorbed, respectively (i.e., $G_{H_2} \simeq 1.2$ and $G_{N_2} \simeq 0.004$).* The total overall reaction equation for the radiolytic N_2 production is given as:

$$2HNO_3 = N_2\uparrow + \frac{5}{2}O_2\uparrow + H_2O.$$

Thus for uranyl nitrate solution, the radiolytic gas is composed of primarily H_2, O_2, N_2 and gaseous fission products such as iodine, xenon, krypton and bromine. As discussed above, the radiolytic yield of H_2 is considerably higher than that of N_2. The gaseous fission products constitute an important health hazard by increasing the radioactivity of the gas. However, they have no significant influence on the radiolytic gas evolution. Finally, considering the above overall reaction equation for the radiolytic N_2

* G value is used to denote radiation chemical yield. It expresses the number of product molecules formed for each 100 eV of energy absorbed by the system.

production and also taking into account the fact that O_2 is a reactive gas, it may be assumed that O_2 does not contribute to the radiolytic gas evolution as much as H_2. Hence it is generally accepted that H_2 is the most important gas contributing to the radiolytic gas phenomenon.

If the liquid superheat is not sufficient for boiling, the gas microbubbles condense into smaller bubbles having an equilibrium size[28),(32)]. These smaller microbubbles are filled mostly with radiolytic gas but they also contain some vapor providing a partial pressure corresponding to the liquid temperature. Thus the equilibrium radius is dictated by the partial gas pressure inside the bubble and the temperature of the liquid. The stability requirement for a gas bubbles in a gas supersaturated solution may be given by

$$p_g + p_v = p_l + \frac{2\sigma}{r_{eq}}. \tag{3.3}$$

Here, p_g and p_v represent the partial pressure (Pa) of gas and vapor inside the bubble, respectively, p_l is the ambient liquid pressure (Pa), σ is the surface tension (N/m), and r_{eq} is the equilibrium radius (m). At room temperature, the vapor partial pressure, p_v, is small and therefore negligible. The gas partial pressure, p_g, dominates the total pressure inside the bubble. As the liquid temperature increases, the partial pressure of vapor also increases. Consequently, according to Equation (3.3), radiolytic gas can form bubbles of equilibrium radius with much smaller partial gas pressure contributions.

Henry's law may provide a good approximation for the partial pressure of gas [33),(34)]. Henry's law states that the mole fraction of a solute dissolved by a given solvent is proportional to the vapor pressure of the solute with which it is in equilibrium at constant temperature. Hence the pressure inside a bubble can be written in terms of the mole fraction of the gas as

$$p_g = K X, \tag{3.4}$$

where K is the Henry's constant (Pa/mole fraction). This constant is temperature dependent. The mole fraction of the , X , can be calculated using[35)]

$$X = \frac{\mathbf{N}}{\mathbf{N} + \sum_i \mathcal{N}^i}, \tag{3.5}$$

where $\sum_i \mathcal{N}^i$ is the total number of moles of all components except the radiolytic gas.

Henry's law is applicable when solubility is small. At moderate pressures, most gases exhibit low solubility in typical liquids.* Also Henry's law is not applicable for systems having very high pressures or very low temperatures[34]. During fast transients, however, high pressures can arise with a significant departure from the ideal behavior of the gas-liquid systems. Thus very high pressures accompanying the fission pulses can result in significant deviations from Henry's law.

The result of many experimental studies of transient criticality of fissile liquids (KEWB, CRAC, and SILENE) has shown that the radiolytic gas bubble nucleation is a threshold phenomenon. If the total number of moles of the radiolytic gas, $\mathbf{N}$, is less than a critical value, $\mathbf{N}_{cr}$, solubility of radiolytic gas is not exceeded and these radiolytic gas microbubbles collapse very quickly by dissolving in water. The lifetime of the microbubbles are very short when $\mathbf{N} < \mathbf{N}_{cr}$. As the fission products decompose more water into its constituents, the gas concentration increases. As soon as the critical value, $\mathbf{N}_{cr}$, is reached (i.e., solubility is exceeded), the radiolytic gas nucleates into bubbles. Thereafter, radiolytic gas microbubbles always exist in the liquid with a potential of growing into gas bubbles. The nucleated gas bubbles are initially very small and they do not move due to buoyancy. They grow in time as more radiolytic gas is produced. This growth is driven by the mechanical pressure difference.** After attaining a certain size, the upward forces on the bubble exceed those directed downward and the bubble start moving upwards. The growth continues during the ascent to the free liquid level since the medium is gas supersaturated. The bubbles eventually leave the solution from the upper free surface and the radiolytic gas is continuously removed from the solution in the form of bubbles.

---

* At atmospheric pressure and at room temperature, H_2 exhibit extremely low solubility in water.

** The isothermal growth of a spherical gas bubble can be described by the following Rayleigh-Plesset equation:

$$r\frac{d^2r}{dt^2} + \frac{3}{2}\left(\frac{dr}{dt}\right)^2 + \frac{4\mu_l}{\rho_l r}\frac{dr}{dt} = \frac{1}{\rho_l}\left(p_g + p_v - p_l - \frac{2\sigma}{r}\right)$$

When the liquid temperature increases, the partial vapor pressure also gradually increases causing smaller gas nuclei to become active and consequently helping the production of gas bubbles.

A new lumped parameter model is developed to simulate the movement of gas bubbles. The model assumes that the cylindrical system can be lumped into several axial regions. Time rate of change of the void volume in each axial region can be written as

$$\frac{dV_j^{PD}}{dt} = \Xi_j^{PD} + \dot{V}_j^{in} - \dot{V}_j^{out}, \tag{3.6}$$

where V_j^{PD} represents the volume of bubbles formed by the mechanical pressure difference driven mechanism. The flow rate of moving bubbles are represented as a product of the void velocity and the average cross-sectional area occupied by the void. The volumetric flow rate of void volume entering and leaving the axial region j can be given as

$$\dot{V}_j^{in} = \frac{v_g}{h} V_{j-1}^{PD} \quad \text{and} \quad \dot{V}_j^{out} = \frac{v_g}{h} V_j^{PD}. \tag{3.7}$$

Here, the void moves upward with a velocity of v_g (m/s). Also, V_{j-1}^{PD} is the void volume in the bottom neighbor of region j (m^3), and h is the size of axial nodes (m). The void source term for each axial region may be given by

$$\Xi_j^{PD} = \begin{cases} 0 & if \quad t < t_{cr} \\ \vartheta \mathbf{P}_j \mathbf{N}_j & if \quad t \geq t_{cr} \end{cases} \tag{3.8}$$

where ϑ is the volume of void produced per energy added to the system per number of moles of radiolytic gas (m^3/J·mol), $\mathbf{P}_j$ is the power in region j (J/sec), and t_{cr} corresponds to time when $\mathbf{N}$ reaches $\mathbf{N}_{cr}$. Hence if the total number of moles of radiolytic gas over the whole region is less than $\mathbf{N}_{cr}$, the void source term is assumed to be zero as shown in Equation (3.8). No threshold is used after $\mathbf{N}$ exceeded $\mathbf{N}_{cr}$ for the first time (i.e., for the fission pulses succeeding first pulse).

Spiegler, Bumpus, and Norman investigated the nucleation radius of gas bubbles during KEWB series of experiments[32]. It was suggested that the gas bubbles nucleate at a fixed radius of 5×10^{-6} m regardless of temperature, liquid pressure, surface tension, dissolved gas concentration, and uranium concentration. By substituting this value into

Equation (3.3), using Henry's Law, and incorporating an appropriate model to estimate the liquid pressure, an approximate value for $\mathbf{N}_{cr}$ may be calculated. Hence when $\mathbf{N}$ is smaller than $\mathbf{N}_{cr}$, the radiolytic gas dissolves in the liquid and microbubbles do not grow as gas bubbles. The number of moles of the radiolytic gas in region j and may be calculated as

$$\frac{d\mathbf{N}_j}{dt} = \mathcal{G}\mathbf{P}_j + a\left\{\dot{V}_j^{in} - \dot{V}_j^{out}\right\}, \tag{3.9}$$

where $\mathcal{G}$ is the produced number of moles of the radiolytic gas per unit energy (mol/J) and a is the number of moles of radiolytic gas per unit void volume (mol/m^3) [36].

According to CRITEX model, the gas bubbles are born at power peaks [8]. Upon the attainment of the moving size, they are small and their upward velocity is slow. As bubbles grow due to expansion and agglomeration, the buoyancy force acting on the bubble increases and they move faster. Hence void velocity is smaller when the power is decreasing, and it is larger, when the power is rising. The void velocity changes as the bubble size changes where the average size of the radiolytic gas bubbles present in the system oscillates following the trend in the power oscillations. CRITEX code adapted a two-speed approach to consider this effect. CRITEX assumes that the void velocity is small (1.5×10^{-2} m/s) when the power is decreasing, and it is larger (3.0×10^{-2} or 4.0×10^{-2} m/s) when the power is rising. This approach successfully reproduced the oscillatory behavior of power for many CRAC and SILENE experiments. However, since the void velocity is switched from one value to another at local power maxima and minima points, the CRITEX estimated power shapes show a factitious shark-fin pattern. In reality, the void velocity has to change continuously as a function of the bubble size. In this study, the following expression is developed as an attempt to represent the void velocity of radiolytic gas bubbles with a continuous function

$$v_g = v_{g0} + sign(\omega)\,\gamma\,\ln(1+|\omega|), \tag{3.10}$$

where the function $sign(\omega)$ is equal to -1, 0, and 1 for $\omega<0$, $\omega=0$, and $\omega>0$, respectively. Equation (3.10) provides an approximate expression for the radiolytic gas bubble velocity as a function of inverse period, ω. Inverse period is a measure of how fast the power changing. Also, the system power is increasing and decreasing depending on whether ω is positive or negative. Therefore, Equation (3.10) is also consistent with the

two-velocity approach of the CRITEX code. In Equation (3.10), v_{g0} is the velocity corresponding to $\omega = 0$ and γ is a tuning constant.

3.4. Boiling

During realistic accident scenarios, the solution temperature may rise above saturation temperature providing sufficient superheat for the onset of boiling[24]. Boiling complicates the modeling of the system since it is not possible to predict the nucleation sites and their distribution. Nucleation sites are the locations where vapor phase develops with less free energy required than in the bulk [37]-[39]. In a fuel solution system, the cavities on the walls of the vessel can be identified as nucleation sites for heterogeneous nucleate boiling. Moreover, microscopic bubbles formed by the passage of fission products may become active producers of vapor bubbles resulting in homogeneous nucleation. Void production cycle also includes bubble growth, departure, and movement which further complicate the modeling of the system. Therefore, there are many variables which enter the boiling process and it is extremely difficult to estimate, within reasonable accuracy, the void production and heat loss rates due to boiling [40]-[42].

One way of treating this problem is to assume a simple sequence of well ordered events representing a boiling system and simulate these event using appropriate correlations and equations available in the open literature. TRACE code assumes that the system is in metastable state during boiling where the liquid phase is superheated. After the solution temperature reaches the saturation temperature, TRACE code calculates the liquid superheat. In a superheated liquid containing radiolytic gas, bubbles smaller than a definite critical size decreases to equilibrium size. The bubbles which exceed the critical size continues to expand. The critical size is dictated by temperature and the mass of the radiolytic gas present in the system and is reached when the pressure due to surface tension plus the liquid pressure equal to the pressure inside the bubble. As discussed before, the pressure inside the bubble is the sum of the partial pressures of radiolytic gas and vapor. Fundamental equilibrium relation for a free spherical bubble containing radiolytic gas and vapor in a large body of uniformly superheated liquid can be given by Equation (3.3). Also,

the following Clausius-Clapeyton relation may be used to connect pressure difference to the difference in temperatures inside and at large distance from the bubble surface [37]:

$$\frac{dT}{dp} = \frac{T v_{lv}}{h_{lv}}, \tag{3.11}$$

where v_{lv} and h_{lv} are the differences between the saturated vapor and saturated liquid specific volumes (i.e., $v_{lv} = v_l - v_v$) and enthalpy (i.e., $h_{lv} = h_l - h_v$), respectively. Combining Equation (3.3) and (3.11) gives the following expression for the superheat in terms of the equilibrium radius[37]:

$$\Delta T_{sup} = T_{sat} \frac{v_{lv}}{h_{lv}} \left\{ \frac{2\sigma}{r_{eq}} \frac{\rho_l}{\rho_l - \rho_v} - p_g \right\}. \tag{3.12}$$

This expression provides an estimate for the magnitude of the liquid superheat ΔT_{sup} required to form a bubble with a radius, r_{eq}, which is in equilibrium with the liquid medium. The bubbles start growing, if r_{eq} and the corresponding ΔT_{sup} is larger than the critical radius and the corresponding critical superheat, respectively. Hence the critical superheat may be defined as the superheat required for the initiation of boiling. Also if cavities on the inner surface of the vessel wall contain entrapped gases with radius greater than the critical radius, nucleation may occur as soon as the temperature exceeds the saturation temperature.

Once the conditions for the initiation of boiling is met in an axial region, the bubble population density has to be calculated. Knowledge on the number and distribution of active nucleation sites is very limited. It was observed that the number of active sites increases as the heat generation rate increases. Since surface tension decreases with increasing pressure, bubble population density can also change with a change in pressure. Finally, measurements for boiling liquids have shown that the bubble population density can be influenced by the superheat. Hence in this work, it is assumed that the bubble population density is a function of heat generation rate, pressure, and superheat and it may be correlated by the expression [42]

$$B = C_1 (S^h)^{e_2} (p_l)^{e_3} (\Delta T_{sup})^{e_4}. \tag{3.13}$$

Here, B is the number of bubble nucleation sites per unit volume (#/m^3), S^h is the heat generation rate per unit volume (J/s·m^3). Also, $\mathcal{C}_1$, $\mathcal{C}_2$, $\mathcal{C}_3$, and $\mathcal{C}_4$ are empirical constants. The bubbles are assumed to be in spherical shape and homogeneously distributed in each axial region.

Three sequential bubble growth modes are assumed to be taking place as time proceeds, namely the initial isothermal hydrodynamic mode, the transition mode, and the advanced isobaric asymptotic mode. For the initial isothermal hydrodynamic mode, bubble growth is governed by liquid inertial forces. In this stage, the bubble diameter is small, bubble growth is fast, and surface tension plays and important role. Forster and Zuber derived the following expression for the bubble radius by solving the extended Rayleigh equation[41]

$$r = \left\{ \frac{16\sigma S^h}{33\rho_l^2 c_l r_{cr} \Delta T_{sup}} \right\}^{1/2} t_b^{3/2}, \tag{3.14}$$

where c_l is a specific heat of liquid. Equation (3.14) assumes a free spherical bubble in an uniformly superheated liquid and bubble starts growing from the critical size. Equation (3.14) apply to pure liquids without chemical impurities and dissolved gases. To be consistent with this assumption, the critical radius, r_{cr}, in Equation (3.14) may be calculated using the simple expression

$$r_{cr} = \frac{2\sigma T}{\rho_v h_{lv} \Delta T_{sup}}. \tag{3.15}$$

The advanced isobaric asymptotic mode is the solution of the heat diffusion problem. In this stage, bubble diameter is relatively large, bubble growth is slow, and surface tension is negligible. Forster and Zuber suggested the following expression to estimate the bubble radius with respect to time for this mode [38]:

$$r = \sqrt{\pi}\,\mathrm{Ja}\left\{ \frac{k_l}{\rho_l c_l} t_b \right\}^{1/2}. \tag{3.16}$$

The growth of vapor bubbles is evaporation driven, and hence the partial pressure of vapor, p_v, dominates over the partial pressure of gas, p_g, with respect to their contribution into the total pressure within the bubble. Even though radiolytic gas is very important as

nucleation sites, it does not contribute significantly to the void volume for this mode. The Jacob number, **Ja**, is defined as

$$\mathbf{Ja} = \frac{\rho_l \, c_l \, \Delta T_{sup}}{\rho_v \, h_{lv}}. \tag{3.17}$$

Also, there is a transition period between these two modes in which our model assumes the smallest calculated radius between Equations (3.14) and (3.16).

As soon as the bubbles reach the departure radius, they start moving upwards. Cole and Rohsenow suggested the following empirical correlation to estimate the departure radius [39]

$$\sqrt{\mathbf{Eo}} = 1.5 \times 10^{-4} \, (\mathbf{Ja}^*)^{5/4}, \tag{3.18}$$

where **Eo** is the Eotvost number and defined as

$$\mathbf{Eo} = \frac{4 \, g \, (\rho_l - \rho_v) \, r_{dep}^2}{\sigma}, \tag{3.19}$$

and $\mathbf{Ja}^*$ is the modified Jacob number and is equal to $\rho_f \, c_f \, T_{sat} \, / \, \rho_v \, h_{lv}$. This simple empirical relation is developed for predicting radius of bubble departure from heated surfaces for water by heterogeneous nucleation. It may also be used to determine the radius when the vapor bubble starts moving upwards in fissile liquids as a crude approximation. As mentioned before, bubbles can also grow unattached to any heating surface by homogeneous nucleation. An equilibrium relation may be used for homogeneous nucleation in which the buoyant force of the spherical bubble has to overcome the inertial and drag (i.e., viscous) forces in the surrounding liquid to be able to start moving upwards. At very low bubble velocities, the drag force (N) may be approximated using Stoke's Law as

$$F_d = 6 \pi \, \mu_l \, v_v \, r_{dep}, \tag{3.20}$$

where v_v is the velocity of vapor bubbles (m/s) and μ_l is the liquid viscosity (Ns/m^2). It is expected that moving vapor bubbles are larger than moving gas bubbles. As a result, they have larger velocities than gas bubbles due to buoyancy. The reader should note that Equation (3.20) is valid up to a Reynolds number close to unity since the inertial effects are ignored in its derivation.

As discussed previously, both homogeneous and heterogeneous boiling can exist during the boiling of fissile liquid in a cylindrical vessel. One of them may be dominant depending on the size and the surface characteristics of the vessel, the superheat, and the equilibrium radius of the radiolytic gas bubbles. Hence modeling the departure phenomenon is very complicated.

In previous experimental boiling studies, it was observed that the bubbles leave a given bubble site at roughly equal time intervals with two periodically repeating phases. The phases are named as growth period and the waiting period where the bubble frequency is defined as

$$f = \frac{1}{Period} \quad \text{where} \quad Period = t_{growth} + t_{wait} \ . \tag{3.21}$$

Prediction of bubble frequency is not well established as yet. Zuber derived the following relation for calculating the bubble frequency[43]

$$2 f r_{dep} = 0.59 \left\{ \frac{\sigma g (\rho_f - \rho_v)}{\rho_f^2} \right\}^m , \tag{3.22}$$

This equation can be solved for f by taking m is equal to 0.25. With f and t_{growth} known, the waiting period, t_{wait}, can be evaluated from Equation (3.21).

Hence it is assumed that identical bubbles appear, grow, and start moving upwards at the same time. During the waiting period, nucleation sites are activated with a critical radius. Vapor bubbles grow from the critical radius to the departure radius. Bubbles then depart and the cycle repeats itself. Following the departure, motion of bubbles can be estimated using the expression

$$\frac{dV_j^{ED}}{dt} = \Xi_j^{ED} + \frac{v_v}{h} \left(V_{j-1}^{ED} - V_j^{ED} \right). \tag{3.23}$$

Here, V_j^{ED} represents the volume of the bubbles formed by the evaporation driven growth mechanism. TRACE assumes that the source term, Ξ_j^{ED}, is equal to zero before the boiling starts and during the bubble growth. Once the departure radius is reached, a new batch of bubbles appear if the liquid superheat is sufficient. The departing void volume is used in Equation (3.23) as the source term, Ξ_j^{ED}. This simple production, growth, and departure

cycle (i.e., simple ebullition cycle) continues as far as the liquid superheat is sufficient to produce bubbles having a radius larger than the critical radius for the initiation of boiling.[1)]

Boiling model described herein is indeed analogous to numerically tracking the lifetime of a single bubble. If this bubble reflects the life cycle of an average bubble, then the same behavior may be assumed for all bubbles in the region during a boiling cycle. Such a simple approach can easily be implemented into a computer code and may represent, in a certain extent, the boiling in a fuel solution system.

TRACE calculates the void volume formed by two different bubble growth mechanisms by solving Equation (3.6) for V_j^{PD} and Equation (3.23) for V_j^{ED}. First mechanism is initiated when the total number of moles of radiolytic gas exceeds the critical value. Second mechanism is initiated when the equilibrium radius exceeds the critical radius for boiling. Therefore, the following conditional formula may be used to express the total void volume for the void reactivity feedback calculations:

$$V_j^{TOT} = \begin{cases} 0 & \text{if } t < t_{cr} \text{ and } r_{eq} < r_{cr} \\ V_j^{PD} & \text{if } t \geq t_{cr} \text{ and } r_{eq} < r_{cr} \\ V_j^{ED} & \text{if } t \geq t_{cr} \text{ and } r_{eq} \geq r_{cr} \end{cases} \tag{3.24}$$

3.5. Surface Evaporation

TRACE can estimate heat and mass losses due to evaporation from the upper free surface. Since superheat is required for the boiling, this superheat can also lead to evaporative heat and mass transfer from the free surface. Evaporation can remove significant amount of water from the system changing the fuel concentration and consequently adding positive or negative reactivity depending on the system under investigation.

From the kinetic theory of gasses, a kinetic equilibrium exists in which a certain number of molecules from the liquid will be replaced by an equal rate of condensing molecules from the vapor. In real boiling process, the kinetic equilibrium is upset by a pressure difference and a net production of vapor is involved from the upper surface.

[1)] It is assumed that bubbles do not grow after departure. In reality, growth continues during the ascent to the top surface. However, this growth is relatively slow.

Assuming that the free liquid surface is at saturation conditions, the net evaporation rate (kg/s) may be given by the following expression[42]:

$$\dot{G}_{evap} = \mathcal{K}\left(\frac{2\pi R_u T_s}{M}\right)^{-1/2}(p_s - p_0)A. \qquad (3.25)$$

Here, R_u is the universal gas constant (J/kg^{-1} mol^{-1} K^{-1}), T_s is the temperature at the free liquid surface (K), M is the molar mass (kg/kg^{-1} mol^{-1}), A is the liquid upper free surface area (m^2), p_s is the saturation pressure (Pa) corresponding to T_s, and p_0 is the saturation pressure (Pa) corresponding to the room temperature. The correction factor $\mathcal{K}$ in Equation (3.25) is known as the coefficient of evaporation. This factor is included for atomic and molecular structures which do not show geometric symmetry. For water, it is equal to 0.04 as recommended by Wyllie. Also the heat flux leaving the surface due to evaporation is equal to $h_{fg}\dot{G}_{evap}$ (h_{fg} is the difference of enthalpy between liquid and gas).

Equation (3.25) represents an idealized case where the liquid evaporates from saturation pressure into a constant ambient pressure. The formulation in Equation (3.25) may not describe surface evaporation well for many real life systems. In real life, the evaporation does not occur over the entire surface simultaneously and the receiving pressure may not stay constant. Hence a correction factor may be introduced in Equation (3.25) as a tuning parameter as an attempt to take these considerations into account.

3.6. Equation of Motion

Acceleration of the fissile liquid and the vessel components may take place during criticality transients, since some momentary uncompensated forces can exist due to sudden nucleation and growth of gas bubbles upon the attainment of the critical gas concentration in the system. Acceleration concerns are important especially for the fissile systems that are less capable of self control such as the plutonium scenarios having a positive temperature coefficient. Considering the fact that the fissile liquid is contained in an open vessel with vertical cylindrical walls, the liquid can expand and move only in vertical dimension (y-axis). If the effects of friction is ignored, Euler equation can be used to relate the velocity in vertical direction to the pressure gradient in that direction:

$$\frac{\partial v_y}{\partial t} = -\frac{1}{\rho}\frac{\partial p}{\partial y} - g, \tag{3.26}$$

where v_y is the velocity along y-axis (m/s) and g is the gravitational acceleration (m/s^2). Locating the center of mass of the cylindrical system at $y = 0$, the total volume of the cylinder is equal to $2yA$ (A is the cross section area of a cylinder). Also, assuming that the whole system can be lumped into one region where the pressure is a linear function of height, Equation (3.26) may be rewritten as:

$$\frac{d^2V}{dt^2} = \frac{4A^2}{m_f}(p - p_0) - 2Ag - \theta_d \frac{dV}{dt}. \tag{3.27}$$

Here, V is the total volume (m^3), p is the pressure at the center of mass (Pa), p_0 is the ambient pressure (Pa), m_f is the total mass of the fissile liquid (kg). The last term in Equation (3.27) is added to account for the momentum dissipation. This term is proposed by David Hetrick[7] where θ_d is an empirical parameter.

Equation (3.27) assumes that the difference between the center of mass and ambient pressures provides the driving force for the equation of motion calculations. Thus this equation requires estimation of the pressure at the center of mass. It is difficult to estimate the pressure since it requires a clear understanding of the pressure mechanism within the system. Sudden introduction of radiolytic gas bubbles upon the attainment of the solubility limit, can create a large pressure increase. According to KEWB work, the amount of gas in the solution may increase 20 times in about 2.0×10^{-4} sec with a speed of 10^5 m^3/s[32]. Since the gas volume is created very rapidly, the fissile liquid can not react to this disturbance fast enough even though the vessel has an open free surface and liquid can freely expand and move in vertical dimension. Growing gas bubbles push the liquid, increasing the liquid density and consequently the pressure. If the pressure difference exceeds the cohesion in liquid, then the system starts moving according to Equation (3.27).

Assuming a simple compressible system, two independent properties will suffice to define the thermodynamic state of the liquid. If we choose these independent properties as the temperature and the density, $p = f(T, \rho)$, the equation of state for the liquid can be written as

$$d\,p = \left(\frac{\partial\,p}{\partial\,T}\right)_{\rho} d\,T + \left(\frac{\partial\,p}{\partial\,\rho}\right)_{T} d\,\rho\,. \tag{3.28}$$

Equation (3.28) leads to the following expression for the pressure change of the center of mass[13]:

$$\delta\,p = \frac{\beta_{VE}}{\kappa}\delta\,T + \frac{\nu}{\kappa}\delta\,\rho\,, \tag{3.29}$$

where β_{VE} is the volumetric expansion coefficient (1/K), κ is the isothermal compressibility (m^2/N), ν is the volume per unit mass (m^3/kg), and the increment, δ represents changes occurring over the time interval, δt. With pressure at time $t - \delta t$ is known, pressure at time t can be calculated as

$$p_t = p_{t-\delta t} + \delta\,p\,. \tag{3.30}$$

Using Equation (3.30), the pressure rise may be modeled as a quasistatic compressive work interaction in which the gas is expanding and pushing the liquid of a constant mass into a smaller volume. Since pressure appears very rapidly, the system may be considered as a closed where the quantity of mass is constant and energy can only cross the system boundaries in the form of work and heat. Note that the quasistatic process assumes that the system is transformed from one equilibrium state to another. This assumption is reasonable if the time required to reach the equilibrium is sufficiently short.

On the other hand, the liquid can also expand due to the open upper free surface. This expansion results in decay of the pressure[32]. This pressure decay may be modeled as a quasistatic expansion work interaction where the liquid having a constant mass and gas volume expanding into a larger volume.

Hence both compression and expansion are taking place in the system simultaneously with different time constants. In this work, a simple model is implemented into TRACE to estimate the pressure by combining the quasistatic compression and quasistatic expansion work interaction models. This pressure model is coupled with the motion model where the TRACE code utilizes the pressure calculated by the pressure model for motion calculations and the volume calculated by the motion model for pressure calculations.

The reader should note that magnitude of the pressure can change depending on the free surface area exists for the radiolytic gas to escape from the system. Operation with limited surface area can increase the pressure significantly especially during fast transients.

3.7. Aerosol Generation

TRACE code also considers the aerosol generation phenomenon using a simple model. Aerosol is a disperse system of liquid and solid particles (fissile liquid in this case) suspended in a gas, usually air. For criticality transients of fissile liquids, bursting of gas/vapor bubbles at the upper liquid surface can generate aerosol droplets. When the gas/vapor bubbles brake at the top surface, significant amount of small particles of the breaking liquid is also carried by the gas/vapor stream. For instance aerosol particles originating from uranyl nitrate solutions consist of uranyl nitrate, fission products, and free nitric acid. These particles pollute the atmosphere in the close vicinity of the vessel by increasing the aerosol concentration. Most of these particles are toxic and they are swept into the respiratory track during inhalation. Since these toxic particles can deposit into the body, they can give rise to undesirable biological effects.

Aerosol generation can originate from several different sources for criticality transients of fissile liquids. When the liquid temperature is very high and the evaporation is very intense, condensing vapors can produce aerosol. The contribution of this source can be neglected at ambient liquid temperatures. Two different mechanisms have been identified for gas/vapor bubbles bursting at the liquid surface, namely, the film drop mechanism and the jet drop mechanism. Film drop mechanism is as a result of gas/vapor bubbles breaking at the liquid surface where bubbles release the gas to the space above the surface while ejecting the liquid on the film cap as a liquid spray. This mechanism is dominant if the radius of the breaking bubbles is larger than 5×10^{-4} m. Film drop mechanism results in small aerosol droplets. Jet drop mechanism, on the other hand, is due to a jet that is projected upwards succeeding a film cap burst. This mechanism results in large aerosol droplets and is the dominant burst mechanism if the breaking bubbles have a radius less than 5×10^{-4} m. For high gas flow rates, the liquid is intensely agitated by the

flowing gas/vapor stream and droplets can also be generated by breakup of liquid filaments and sheets within the bulk itself.

Aerosol production rates are strongly influenced by the gas flow regimes exist in the system. Orht, Epstein, Linehan, Lambert, and Stachyra[44] investigated the flow regimes observed for N_2 gas fed steadily in a pool of the water. Several distinct modes of flow behavior were observed. Gas flow rates up to 2×10^{-2} m/s resulted in ideal bubbly flow where the bubbles rise in the liquid and the individual bubbles break at the liquid surface. At higher flow rates close packing of bubbles were observed and this behavior exited up to bubble velocities 6×10^{-2} to 10×10^{-2} m/s. This phase was named as compact bubbly flow regime. With further increase in the bubble velocity, the flow pattern became unsteady and chaotic. The liquid was agitated by the flowing gas where the close packing of bubbles resulted in the periodic release of a large gas bubble at the top free liquid surface. This flow regime is named as churn turbulent flow.

Since the radiolytic gas bubbles are assumed to be small, it is reasonable to assume that bubbly flow will be dominant with gas bubbles. Vapor bubbles, however, are expected to be larger than radiolytic gas bubbles and both bubbly and churn turbulent flow regimes may exist depending on the bubble velocity which in turn depends on the bubble size. The transition from bubbly flow to churn turbulent flow occurs at a Kutateladze number of $0.325\left(\rho_L / \rho_H\right)^{1/2}$ where ρ_L is the density of lighter phase (kg/m^3) and ρ_H is the density of heavier phase (kg/m^3). This correlation was suggested by Ishii. The Kutateladze number is defined as

$$K = \frac{j_{g,t}\sqrt{\rho_C}}{\left[g\sigma\left(\rho_H - \rho_L\right)\right]}, \tag{3.33}$$

where ρ_C is the density of continuous phase (kg/m^3) and $j_{g,t}$ is the superficial gas velocity (m/s).

The aerosol generation models implemented in TRACE for both gas/vapor bubbles can be summarized as follows. Void volume leaving the top surface over the time interval δt is calculated as

$$\delta V_{top} = v \frac{V_{top}}{h} \delta t, \tag{3.34}$$

where V_{top} is the void volume in the top axial node (m^3). The approximate number of bubble bursts over the time interval δt may be given by

$$\mathcal{B} = \frac{\delta V_{top}}{V_{bub}}. \tag{3.35}$$

For vapor bubbles, the bubble volume, V_{bub}, may be approximated according to the departure radius. Volume of droplets produced can be given by

$$\delta V^{DR} = E \frac{\rho_L}{\rho_H} V_{bub} \mathcal{B}. \tag{3.36}$$

Here, E is the dimensionless entrainment mass flux of droplets for a single bubble. For bubbly flow regime, it may be given as

$$E = \left(\frac{\rho_H}{\rho_L}\right)\left(\frac{V_{fd}}{V_{gb}}\right) \mathcal{F}. \tag{3.37}$$

In Equation (3.37), V_{fd} is the total volume of liquid droplets ejected for each bubble of volume V_{gb} that bursts and $\mathcal{F}$ is the fraction of droplets ejected whose radius is less than a given value. The ratio (V_{fd} / V_{gb}) depends on the liquid and gas properties and also the bubble size. Several empirical estimates for (V_{fd} / V_{gb}) available in the open literature are implemented into TRACE as an option. Also TRACE uses near-surface, momentum-controlled and far-field region correlations to calculate E for the churn turbulent flow regime. The near-surface region is a very narrow region close to the surface where the gas/vapor stream contains all the droplets which pass through this region without reversing the direction. In the momentum-controlled region, the droplets having a terminal velocity larger than the velocity of the gas/vapor stream lose their velocity and fall back into the liquid. The droplets having a terminal velocity smaller than the velocity of the gas/vapor stream are carried to the far field region. Finally, the far-field region correlations provide an estimate for the amount of aerosol material introduced into the room where the vessel is located. For the details of the aerosol generation models used in TRACE, user is referred to References 45, 46, and 47.

4. SIMULATION CODE

A FORTRAN computer code named TRACE (Transient Analysis of Criticality Excursions) has been developed using the models described in Sections 2 and 3. TRACE solves the differential equations using LSODE (Livermore Solver for Ordinary Differential Equations), a package of subroutines for the simultaneous numerical solution of systems described by ordinary differential equations[48]. LSODE was developed by Hindmarsh at Lawrance Livermore National Laboratory to solve the traditional initial value problem for stiff and non-stiff system by calling a used supplied subroutine. This subroutine defines the set of first order differential equations of the form

$$\frac{d\,y(i)}{d\,t} = f(i) = f\left(i,t,y(1),y(2),\ldots,y(neq)\right), \qquad i = 1,2,\ldots,neq \tag{4.1}$$

Here, y is a real array for the vector of dependent variables, t is the independent variable, and neq is the size of ODE system (i.e., number of the first order ordinary differential equations). LSODE uses Adams (predictor-corrector) method for non-stiff systems, and Backward Differentiation Formula (BDF) method for stiff systems[49].[1] LSODE controls the vector of estimated local errors, $\varepsilon = [\varepsilon(i)]$, in y using the following inequality:

$$\left\| \frac{\varepsilon(i)}{ewt(i)} \right\|_{rms} \le 1 \ . \tag{4.2}$$

Here the root-mean-square norm, $\|x\|_{rms}$, is a real positive number which is the measure of the size of all of errors and is defined as

$$\|x\|_{rms} = \sqrt{\frac{\left(\sum_{i=1}^{neq} x(i)^2\right)}{neq}} \ . \tag{4.3}$$

---

[1] A system of ordinary differential equations is said to be stiff if all the eigenvalues of its Jacobian matrix satisfy the following two conditions[49]:

(a) real parts of the eigenvalues are less than zero, and

(b) real parts of the eigenvalues span several orders of magnitude resulting in components that are decaying at widely differing rates.

Also the vector of weights, $ewt = [\, ewt(i) \,]$, is calculated according to the value of the input parameter *itol* as

$$ewt(i) = \begin{cases} rtol \,|y_i| + atol & for \quad itol = 1 \\ rtol \,|y_i| + atol(i) & for \quad itol = 2 \\ rtol(i) \,|y_i| + atol & for \quad itol = 3 \\ rtol(i) \,|y_i| + atol(i) & for \quad itol = 4 \end{cases} \tag{4.4}$$

Here *rtol* is the relative error tolerance parameter (a scalar or an array), *atol* is the absolute error tolerance parameter (a scalar or an array), and *itol* is an indicator for the type of error control.

The size of the ODE system, *neq*, depends on the user-supplied input parameters. TRACE automatically set up the ordinary differential equations for LSODE according to the input parameters defining the calculation options and the number of axial and radial regions.

TRACE consists of three major computational segments. First segment contains the subprograms that are executed only once per program run. This segment includes the initial calculations and the estimation of inherent neutron source strength. Second segment contains the subprograms that are executed only once at every edit interval. These subprograms performs the calculations outside of LSODE, however, their results are coupled with the differential equations solved by LSODE. These calculations include solution of the pressure equation, and the evaluation of the aerosol production, the surface evaporation, and the mass balances. The second segment also includes the calculations for the boiling simulation. Finally the third segment statements conducts the solution of the differential equations using LSODE for the point neutronics, the heat transfer, the gas/vapor bubble movement, and the fluid motion. LSODE solves the differential equations for the integration invervals. The size of the integration intervals are automatically chosen by LSODE within an edit interval. Results are written into output files at each user-supplied output interval. Hierarchy of TRACE time intervals is shown in Fig. 4.1.

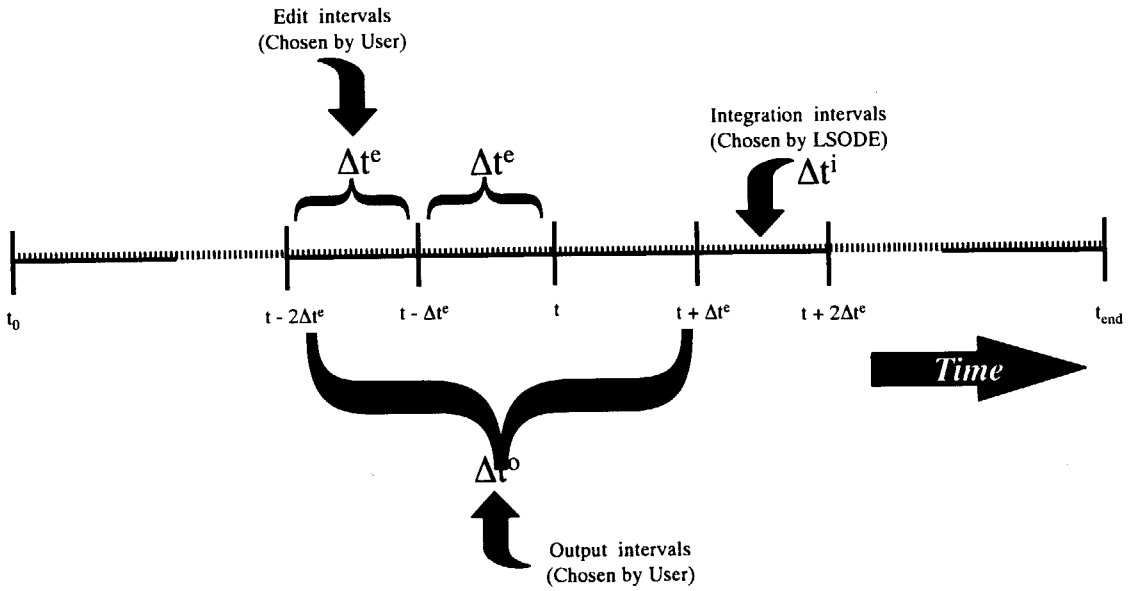

Fig. 4.1 Hierarchy of time intervals in TRACE

The thermodynamic property data required by the calculations are supplied into TRACE by a package of FORTRAN subprograms. This package is developed in parallel to TRACE code and named as NCSELIB (Nuclear Criticality Safety Evaluation Library). NCSELIB consists of several FORTRAN subprograms which utilize equations, polynomial fits, and correlations to estimate property data associated with the system components. It contains functions to calculate free convection heat transfer coefficients for various geometries as described in Reference 16. Property data for saturated water in liquid and gaseous phases, air, and stainless steel are provided as BLOCKDATA routines along with modules to interpolate them for a given temperature (or pressure). NCSELIB also provides physical constants, nuclear data, and conversion factors for TRACE calculations. Furthermore, steam table subprograms STEAMZ, STEAM, STEAMV and their dependency routines are implemented into NCSELIB to calculate the thermodynamic properties of the subcooled water and the saturated steam. These routines were developed by Kobayashi[50] at Japan Atomic Energy Research Institute.

TRACE incorporates the double precision function subprograms DBESJ0 and DBESJ1 to compute the Bessel functions. DBESJ0 calculates the Bessel function of the first kind of order zero, $\mathbf{J}_0(x)$, and DBESJ1 calculates the Bessel function of the first kind

of order one, $J_1(x)$, for a given argument x. These subprograms were developed by Fullerton at Los Alamos Scientific Laboratory.

TRACE can plot the results on the computer screen by a graphical interface as the program runs. This interface is implemented into TRACE using PGPLOT graphics subroutine library. PGPLOT is a FORTRAN callable package of subroutines developed at California Institute of Technology for making simple scientific graphs. In this work, the graphics output is directed to a XWindows device. The following information are shown on the graphics screen and updated periodically at every user-supplied output interval

- time, average temperature and total number of fissions,
- axial and radial temperature distribution of the fissile liquid (using a color coded temperature scale),
- axial void volume distribution (using a gray scale coded void scale),
- plots of external, feedback and total reactivities versus time,
- plot of system power versus time (TRACE can also plot total fissions, temperature, or pressure instead of system power according to a user-supplied flag),
- indicators for the solution feed or transient rod movement,
- height of the solution relative to a scaled ruler.

Fig. 4.2 shows the main program loop of TRACE. Appendix serves as a user's guide for TRACE. It contains brief description of the TRACE subprograms, the general input, and the I/O files. The code is currently running on a SUN-SPARC workstation at the Department of Fuel Cycle Safety Research of Japan Atomic Energy Research Institute.

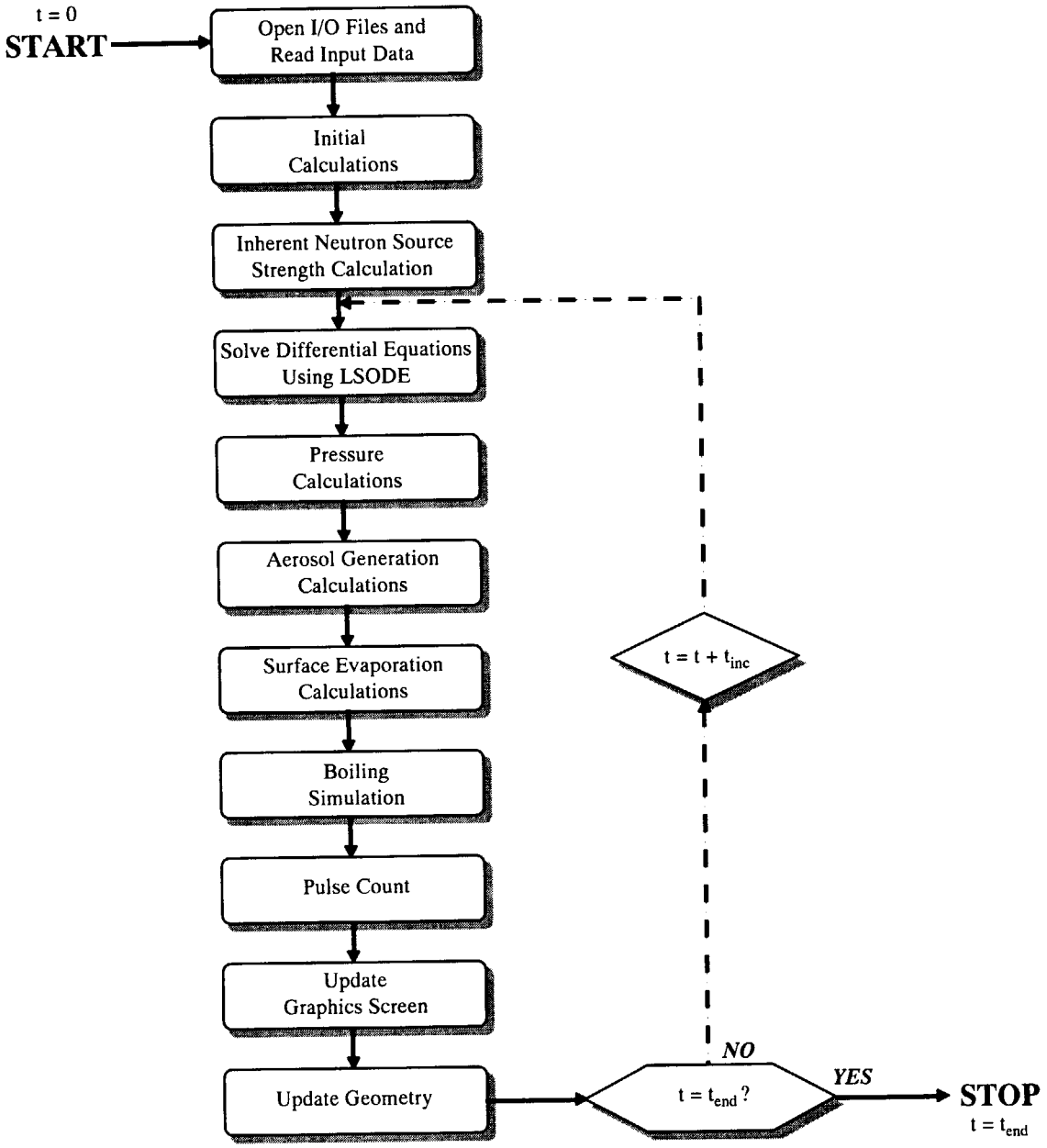

Fig. 4.2 Main program loop of TRACE.

5. RESULTS

5.1. Introduction

To evaluate the models described in Sections 2 and 3, several CRAC experiments are calculated using the TRACE code. CRAC experiments were performed by Commissariat a l'Energie Atomique (CEA) using aqueous solutions of uranyl nitrate[4]. The uranium was 93% enriched in ^{235}U. During these experiments criticality excursions were observed for a wide range of solution concentrations and reactivity addition rates, The excursions were initiated by injecting aqueous uranyl nitrate solutions into 300-mm and 800-mm-diam cylindrical containers to height in excess of the critical height.

Thirteen CRAC experiments are considered in this work for evaluation of the new simulation code. Tables 5.1 and 5.2 summarize the critical data and the excursion data, respectively, for these experiments[51]. The vessel diameter, the critical height ($\mathbf{H_c}$), the acid molarity, the uranium concentration, and the concentration of ^{235}U are tabulated in Table 5.1. Also Table 5.2 shows the final height ($\mathbf{H_f}$), the time required for $\mathbf{H_f - H_c}$ addition, the rate of solution addition, the rate of initial ramp reactivity increase, and the excess above critical height. A short description of each experiment is provided in following subsections along with the TRACE simulation results. The power curves are provided for each experiment where the experimental and the calculated results are shown on the same graph for comparison.

Previous experimental studies have shown that several distinct regions can be identified on the power curves of fissile liquid criticality transients. These regions may listed as:

- first fission pulse,
- power oscillations,
- non-boiling plateau, and
- boiling plateau.

If the reactivity addition rate is sufficiently large, high rate of energy will be released in a very short time for the first fission pulse. This first power peak with a very short initiation period is commonly named as the spike. The spike is important since it

Table 5.1

Summary of Critical Data for Experiments That were Analyzed with TRACE code.

Experiment	Vessel Diameter (cm)	Critical Height H_c (cm)	Acid Molarity (N)	Uranium Concentration (g/liter)	^{235}U Concentration (g/liter)
CRAC01	30	191.30	2.00	52.0	48.4
CRAC05	30	69.05	2.10	61.1	56.9
CRAC08	30	27.25	2.23	202.0	188.0
CRAC09	30	42.90	2.00	78.3	72.9
CRAC12	30	43.53	1.95	77.9	72.5
CRAC16	30	42.00	2.20	82.3	76.6
CRAC18	30	41.97	2.00	79.6	74.1
CRAC20-4	30	27.10	2.32	218.0	203.0
CRAC20-5	30	27.10	2.32	218.0	203.0
CRAC22	30	26.91	2.07	207.0	193.0
CRAC37	80	45.00	2.00	21.8	20.3
CRAC50	30	40.50	2.05	80.9	75.2
CRAC52	30	40.41	2.18	84.3	78.4

Table 5.2

Summary of Excursion Data for Experiments That were Analyzed with TRACE code.

Experiment	Final Height H_f (cm)	Time for H_f - H_c Addition (s)	Rate of Fuel Addition (liter/h)	Rate of Reactivity Addition ($/s)	Excess Above Critical Heig. H_f - H_c (cm)
CRAC01	371.4	304	1440	0.00341	180.1
CRAC05	100.4	51	1483	0.0667	31.4
CRAC08	32.8	8	1622	0.746	5.6
CRAC09	55.3	19	1594	0.247	12.4
CRAC12	62.8	451	104	0.0156	19.3
CRAC16	82.1	205	466	0.0755	40.1
CRAC18	102.4	1404	104	0.0168	60.4
CRAC20-4	30.6	5	1489	0.685	3.5
CRAC20-5	33.0	11	1340	0.616	5.9
CRAC22	33.3	15	1066	0.501	6.4
CRAC37	52.1	282	448	0.016	7.1
CRAC50	63.2	94	511	0.136	22.7
CRAC52	64.8	98	552	0.134	24.4

determines the severity and the immediate consequences of accidents (such as radiation dose to the personnel before emergency evacuation). The peak value of the spike can change significantly with respect to the rate of reactivity addition. For very large reactivity addition rates, size of the spike may increase tremendously in a very short time. The spike is controlled and terminated by thermal effects and also by production of radiolytic gas.

If the reactivity addition rate is sufficiently low, the initiation period of the first fission pulse will be long and the first fission pulse will have a small peak power. Such excursions are named as Low Power Criticality Accident (LOPCA).

Following the spike, in general, a series of fission pulses are observed. If the vessel continues to fill, this will add reactivity into the system. Also, the radiolytic gas bubbles (generated as a result of energy release in the power peaks) move upwards and leave the solution from the upper free surface. Removal of gas bubbles can also provide a strong reactivity feedback. Therefore, generation and removal of radiolytic gas as well as continuous addition of fissile liquid into the vessel are responsible for generating the power oscillations following the spike. This oscillations, in general, show a decreasing power amplitude.

SHEBA experiments have shown that in LOPCA type transients no detectable power oscillations take place as a result of radiolytic gas evolution. For LOPCA, power oscillates with long period due to thermal cycling.

The power generated in the solution increases the system temperature as the time proceeds. Parallel to this increase in temperature, excess reactivity driving the power oscillations balances and leaves a steady-state power shape behind while the temperature of the fissile liquid is still less than the boiling temperature. This steady-state region on the power curve is termed as "non-boiling plateau" in this report. Power in non-boiling plateau gradually decreases as temperature increases.

If sufficient thermal energy is released, temperature of the fissile liquid can rise above the boiling temperature. As the boiling phase is attained, oscillatory nature of the system gradually dampen to a steady state condition. Since water is removed from the system by boiling and also by surface evaporation, power may increase slightly if reactivity feedback coefficient with respect to change in fuel concentration is positive. The sign of the

reactivity feedback coefficient due to water removal (and the corresponding uranium concentration increase) depends on the fuel concentration. Thus the water removal by boiling may as well add positive reactivity into the system (as in CRAC 16 experiment). This power shape due to boiling is termed as "boiling plateau".

The boiling can continue for some time increasing the fuel concentration as water is removed. Power gradually adjust itself to the changes in fuel concentration. Eventually enough water is removed from the system such that the system can no longer maintain criticality. From that time on, the fission rate declines as liquid is removed from the system. The power level for boiling plateau is important since the radiation field is a function of power level for long-duration-continuing type transients.

Therefore, the quantities of most interest in this work are the spike size, time location of spike, the power level of the non-boiling and boiling plateau, and the power in the oscillating phase. These quantities studied using TRACE for each of the thirteen CRAC experiments considered in this work and the results are reported in the following subsections. The external reactivity, the temperature reactivity feedback, and the void reactivity feedback functions are adopted from AGNES report[52] for CRAC 01, 05, 08, 09, 12, 20-4, 20-5, and 22 experiments. On the other hand, these functions are calculated in this work using the procedure described in Section 2 for CRAC 16, 18, 37, 50, and 52 experiments. Moreover, reactivity feedback function due to change in fuel concentration is estimated and used in the simulation studies for some of the experiments listed above (such as CRAC 16). For all simulations in this report, the fissile system is assumed to be at delayed critical condition at time zero.

The values of several parameters are adjusted to obtain the best agreement with the experimental results. These parameters can be listed as

- quantities C_j-value and the ϑ-value for the void generation model,
- quantities v_{g0} and γ for the new void velocity model,
- empirical constants, C_1, C_2, C_3, and C_4, for the bubble population density calculations.

These parameters can influence the timing and the magnitude of the quantities calculated by TRACE. The empirical constants for the bubble population density determines the power level for the boiling plateau.

Moreover, parametric studies have shown that, if the spike size is several orders of magnitude larger than the subsequent fission pulses, the void velocity has to be adjusted for some of the above listed experiments. This adjustment is done by multiplying the void velocity by a correction factor for the time interval between the spike and the second fission pulse.

The following listed parameters are also adjusted to obtain a satisfactory fit with the experiments, but such adjustments are done only when it is absolutely necessary:

- initial power, $\mathbf{P}_0$,
- initiation time, t_{init}, for the first persistent fission chain,
- reactivity, ρ_0, at time zero.

The values of adjusted parameters are provided for each experiment in succeeding subsections. The initial reactivity, ρ_0, is assumed to be zero if it is not stated otherwise for the following set of experiments.

5.2. CRAC 01 Experiment

CRAC 01 experiment was conducted in a 300-mm-diam cylindrical vessel containing 93% enriched uranyl nitrate solution with a uranium mass of 6.75 kg (6.28 kg of ^{235}U mass). Solution height at start of solution addition was 186.1 cm. The system was at subcritical condition. Solution was added into the system at a rate of 1440 liter/h (4.00×10^{-4} m^3/s). This addition resulted initially in a uniform ramp reactivity increase of 0.00341 \$/s. Because the reactivity addition rate was very slow, it is expected that the conventional point kinetics should provide a satisfactory estimate for the first power pulse.

In CRAC 01, the system reached the critical height 191.3 cm in 8.8 seconds. Following criticality, solution addition continued 304.2 seconds until the height reached 371.4 cm. The experiment is ended in approximately 260 minutes. The first fission pulse was observed 232 seconds after system reached delayed critical with a peak power of 1.1×10^{16} fissions/s.

Figure 5.1 shows the computer simulation of CRAC 01 system power for the first 900 seconds. As can be seen in this figure, there is a reasonable agreement between the calculations and the experiments. The code estimates the first fission pulse as 1.22×10^{16} fissions/s. The time to the peak from delayed critical is predicted as 210 s. TRACE estimates the total inherent neutron source strength of CRAC 01 at the delayed critical as 614 neutrons/s.

Power oscillations as a result of radiolytic gas evolution was essentially not existed for CRAC 01. The oscillation occurred in long term are attributed to thermal cycling phenomenon. This thermal cycling phenomena is not, at present, modeled with TRACE. For the simulation results shown in Fig. 5.1, a G -value of 1.466×10^{-8} mol/J and a ϑ -value of 1×10^{-8} m^3/J·mol are used to model the radiolytic gas phenomenon. No initiation time is used for the neutronics modeling. Also the initial power is assumed to be small.

5.3. CRAC 05 Experiment

CRAC 05 experiment was conducted using a 300-mm-diam cylindrical vessel. This experiment has been frequently used for validation studies of computer codes (i.e., AGNES, CREST, and SKINATH-AR). The fuel was 93% enriched uranyl nitrate solution with an uranium mass of 2.88 kg (2.68 kg of ^{235}U mass). The uranium concentration was relatively low (52 g/liter). The acidity and the NO_3^- molarity of the fissile liquid was 2.1 N and 2.62 N, respectively. Solution height at start of solution addition was 13.23 cm and the system was at subcritical condition. Solution was added at a rate of 1483 liter/h (4.12×10^{-4} m^3/s) . This addition resulted initially in a uniform ramp reactivity increase of 0.0667 \$/s. The system reached the critical height 69.05 cm in 14.8 seconds. Following criticality, solution addition continued for about 106.2 s. The final solution height was 100.40 cm. The experiment ended in approximately 19 minutes.

The first fission pulse was observed 21.5 seconds after delayed criticality with a peak power of 6.3×10^{16} fissions/s. Figure 5.2 shows some comparisons between the experimental and TRACE calculated results for CRAC 05. As can be seen in this figure, TRACE reproduces the first 5 fission pulses and the gradual decrease in power peaks quite well. There is a good agreement with regard to the size of the first power peak. The code

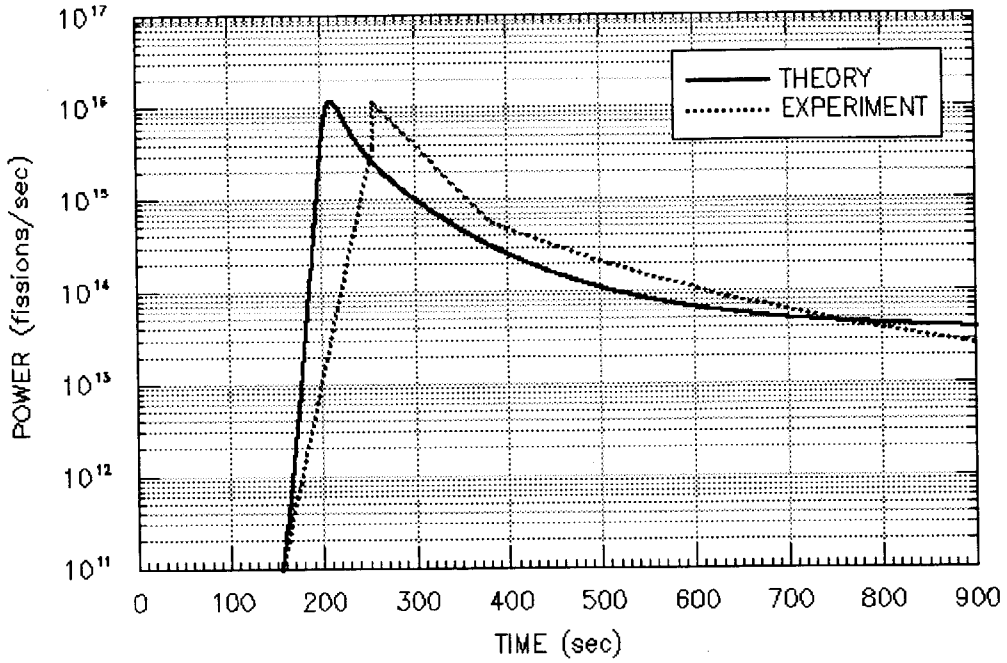

Fig. 5.1 Power versus Time: Comparison of TRACE Results with Experimental Results for CRAC 01

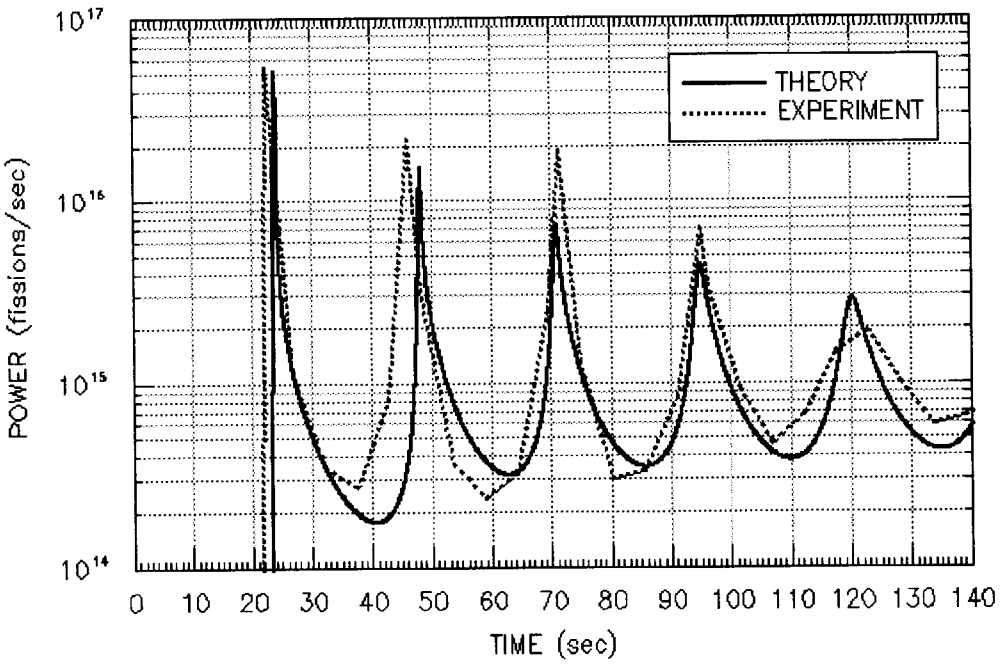

Fig. 5.2 Power versus Time: Comparison of TRACE Results with Experimental Results for CRAC 05

predicts the first fission pulse as 5.21×10^{16} fissions/s. The time to the peak from delayed critical is estimated as 23.8 s.

The quantities v_{g0} and γ are taken to be 0.039 m/s and 0.2, respectively. Also, the G-value is equal to 1×10^{-7} mol/J and the θ-value is equal to 6×10^{-7} m^3/J·mol for the modeling of radiolytic gas effects. The initial power is assumed to be very small. No initiation time is utilized for the simulation of the initial rise in neutron population. TRACE estimates the total inherent neutron source strength of this experiment as 260 neutrons/s.

5.4. CRAC 08 Experiment

CRAC 08 experiment considers a criticality transient involving 93% enriched uranyl nitrate solution with an uranium mass of 3.81 kg (3.55 kg of ^{235}U mass). The acidity and the NO_3^- molarity of the fissile liquid was 2.23 N and 3.95 N, respectively. The uranium concentration was relatively higher in this experiment (202 g/liter).

CRAC 08 experiment continued approximately 10 minutes. Solution height at start of solution addition was 10.04 cm where the system was at subcritical condition. Solution was added into the system at a rate of 1622 liter/h (4.50×10^{-4} m^3/s). This addition resulted initially in a uniform ramp reactivity increase of 0.746 $/s. Thus the reactivity addition rate was relatively fast. The fissile system reached the prompt critical condition in less than 2 seconds

In CRAC 08, the system attained the critical height 27.25 cm in 25.8 seconds. Following criticality, solution addition continued 8.2 s more until the solution height reached 32.8 cm. The first fission pulse was observed 3.41 seconds after delayed criticality with a peak power of 3.0×10^{19} fissions/s. The spike size was large as a result of large reactivity addition rate.

The power calculated by TRACE for CRAC 08 is compared to the experimental results in Fig. 5.3. The code predicts the first fission pulse as 1.73×10^{19} fissions/s where the time to the peak from delayed critical is estimated as 3.41 s. The new void velocity model is used in the simulation where the quantities v_{g0} and γ are assumed to 0.016 m/s and 0.01, respectively. For the TRACE results shown in Fig. 5.3, the G-value and the θ-

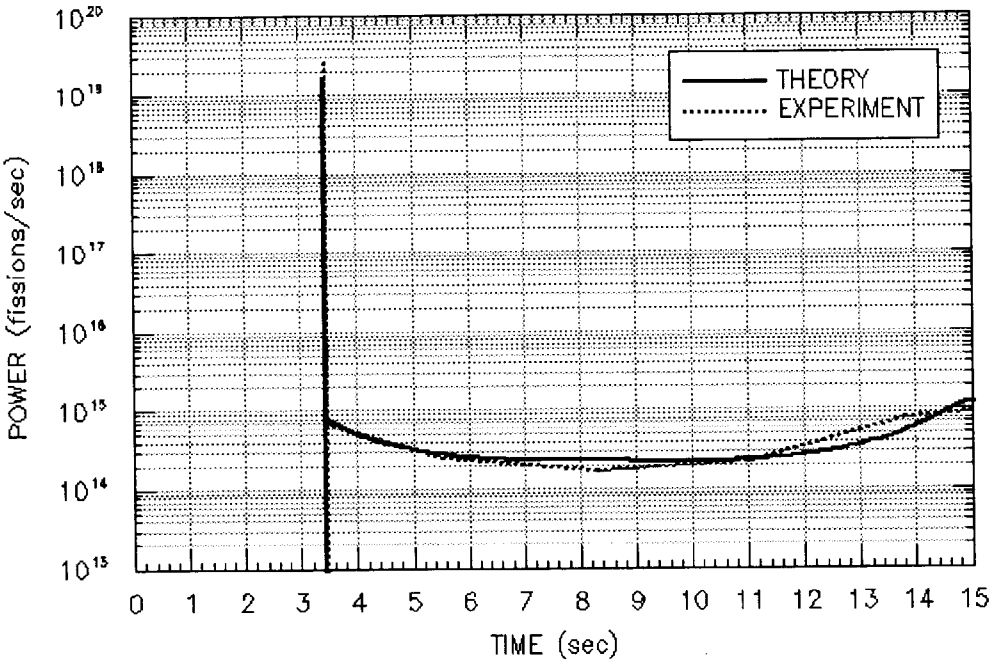

Fig. 5.3 Power versus Time: Comparison of TRACE Results with Experimental Results for CRAC 08

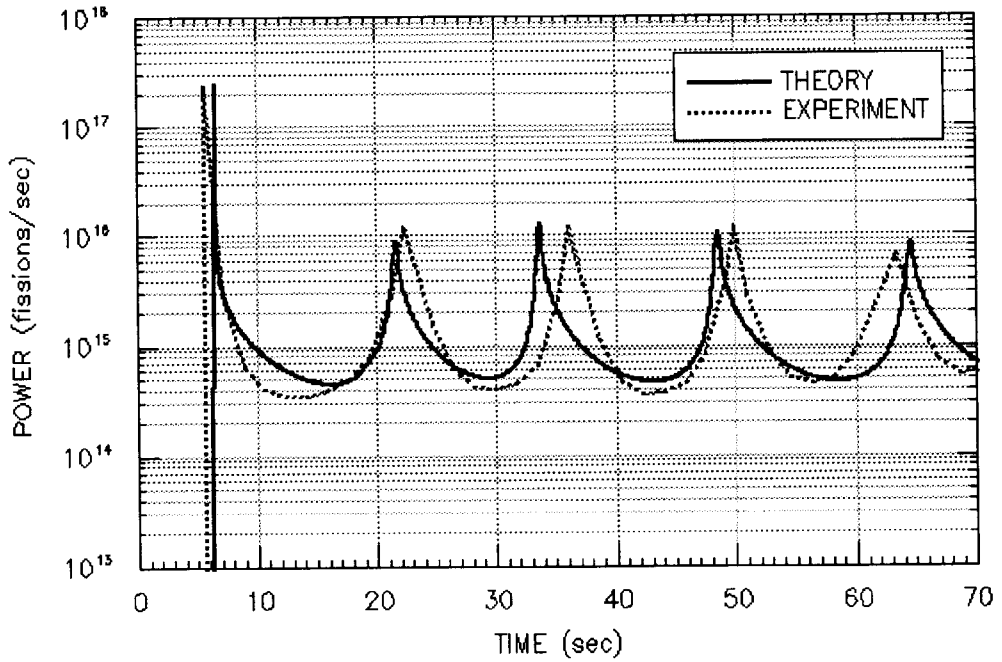

Fig. 5.4 Power versus Time: Comparison of TRACE Results with Experimental Results for CRAC 09

value are equal to 1.8×10^{-7} mol/J and 1×10^{-6} m^3/J·mol, respectively. TRACE estimates the total inherent neutron source strength of CRAC 08 as 320 neutrons/s. The initiation time is taken as 3.4 s, which is obtained by Eq. (2.21). The initial power is assumed to be very small.

5.5. CRAC 09 Experiment

CRAC 09 experiment considered a criticality transient involving 93% enriched uranyl nitrate solution with an uranium mass of 2.31 kg (2.15 kg of ^{235}U mass). The acidity and the NO_3^- molarity of the fissile liquid was 2.0 N and 2.67 N, respectively. This experiment continued approximately 6 minutes. The initial solution height was 10.10 cm. The system was at subcritical condition at start of solution addition. Solution was added into the system at a rate of 1594 liter/h (4.43×10^{-4} m^3/s). This addition resulted initially in a uniform ramp reactivity increase of 0.247 \$/s. The system reached the critical height 42.90 cm in 50.1 seconds. Following criticality, solution addition continued 18.9 s until the height reached 55.3 cm.

The first fission pulse was observed 5.4 seconds after delayed criticality with a peak power of 2.9×10^{17} fissions/s. Figure 5.4 presents the experimental results and results from TRACE for the first 5 fission pulses. TRACE accurately predicts the first power pulse as 2.55×10^{17} fissions/s where the time to the peak from delayed critical is estimated as 6.4 s. The succeeding 4 pulses are also estimated with a satisfactory accuracy. The difference between the experimental and the TRACE calculated results are quite small. TRACE predicts the total inherent neutron source strength of CRAC 09 as 205 neutrons/s.

The new velocity model is employed in the simulation for modeling the radiolytic gas effects. The quantities v_{g0} and γ are taken as 0.021 m/s and 0.09, respectively. For simulation results shown in Fig. 5.4, the G-value and the θ-value are equal to 6×10^{-7} mol/J and 1×10^{-7} m^3/J·mol, respectively. The initial power is assumed to be very small. Also no initiation time is used for the neutronics modeling.

5.6. CRAC 12 Experiment

CRAC 12 experiment considered a criticality transient involving 93% enriched uranyl nitrate solution with an uranium mass of 2.33 kg (2.17 kg of ^{235}U mass). The acidity and the NO_3^- molarity of the fissile liquid was 1.95 N and 2.61 N, respectively. This experiment continued approximately 17 minutes. Solution height at start of solution addition was 9.98 cm where the system was subcritical. Solution was added into the system at a rate of 104 liter/h (2.89×10^{-5} m^3/s). This addition resulted initially in a uniform ramp reactivity increase of 0.0156 \$/s. The system reached the critical height 43.53 cm in 788 seconds. Following criticality, solution addition continued 451 seconds until the height reached 62.8 cm.

The first fission pulse was observed 65 seconds after delayed criticality with a peak power of 1.0×10^{16} fissions/s. The power curve calculated by TRACE code is compared to the experimental results in Fig. 5.5. As may be observed from this figure, TRACE code does quite well for the first 400 seconds. The first fission pulse is lower than the experiment, however, its timing is almost exact. The code predicts the first fission pulse as 2.27×10^{15} fissions/s where the time to the peak from delayed critical is estimated as 66 s. The new velocity model is employed in the simulation where the quantities v_{g0} and γ are assumed to 0.035 m/s and 0.08, respectively. The initial power is assumed to be very small. Also, a G -value of 7.3×10^{-6} mol/J and a θ -value of 1×10^{-8} m^3/J·mol are used for the modeling of radiolytic gas effects. No initiation time is used for the modeling of initial power rise. TRACE calculates the total inherent neutron source strength of this experiment as 207 neutrons/s.

5.7. CRAC 16 Experiment

CRAC 16 experiment considers a criticality transient involving 93% enriched uranyl nitrate solution with an uranium mass in the solution of 2.37 kg (2.21 kg of ^{235}U mass). The acidity and the NO_3^- molarity of the fissile liquid was 2.2 N and 2.90 N, respectively. This experiment continued approximately 13 minutes.

In CRAC 16, the system was at critical condition at low steady power when the ramp addition was initiated system at a rate of 466 liter/h (1.29×10^{-4} m^3/s). This addition

resulted initially in a uniform ramp reactivity increase of 0.0755 $/s. Since this experiment was started from low steady power, the initial neutron source strength was relatively high. This resulted in a smaller spike size. The height at start of solution addition was 42 cm. Solution addition was continued 205 seconds until the height reached 82.1 cm. The first fission pulse was observed 10 seconds after start of solution addition. The size of the spike was 1.6×10^{16} fissions/s.

In this experiment, the fissile liquid reaches the boiling temperature approximately 5 minutes after delayed criticality. The experimental power curve for CRAC 16 shows an oscillating pattern until the saturation temperature is reached. After the onset of boiling, the sharp power pulses are damped to a steady power pattern. The power level was approximately 4×10^{14} fission/s for the boiling plateau. Power slightly increased in boiling phase, since boiling and surface evaporation remove water from the system.

The evaluation of the new boiling model is accomplished by comparing results obtained with TRACE with CRAC 16 experimental results for the boiling region. TRACE is executed for the full time range of the available experimental data. The results are shown in Fig. 5.6. As seen in this figure, the new simulation code predicts the initial oscillatory behavior and the time location of the onset of boiling quite good. The new velocity model is employed in the simulation. The quantities v_{g0} and γ are assumed to 0.02 m/s and 0.076. Also, a G-value of 8×10^{-8} mol/J and a ϑ-value of 1.1×10^{-7} m^3/J·mol are used for the modeling of radiolytic gas effects. Because the system was at low steady state power when the ramp reactivity addition was started, the initial power is assumed to be large. No initiation time is used for the neutronics modeling. The empirical constants, C_1, C_2, C_3, and C_4, for the bubble population density are taken as 1.1×10^{-11}, 3, 0, and 0, respectively. These values are estimated by a parametric study.

The code predicts the first fission pulse as 2.07×10^{16} fissions/s where the time to the peak from delayed critical is estimated as 11.3 s. Moreover, the power in the boiling plateau is also in satisfactory agreement with the experiment. Power increases as boiling and surface evaporation removes water from the system. As a conclusion, TRACE estimates the general behavior of the boiling systems quite well.

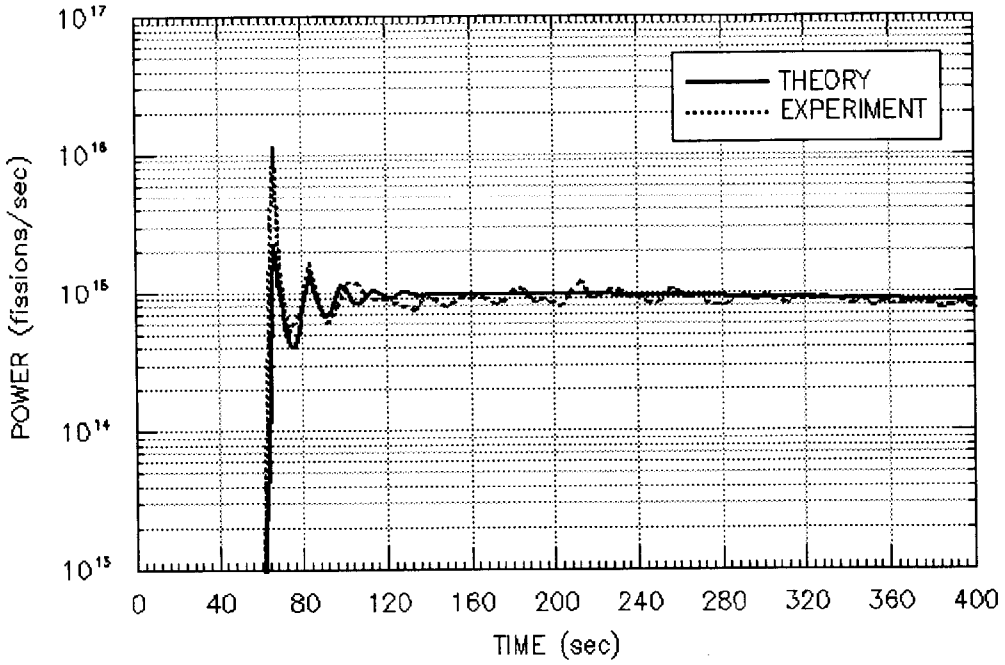

Fig. 5.5 Power versus Time: Comparison of TRACE Results with Experimental Results for CRAC 12

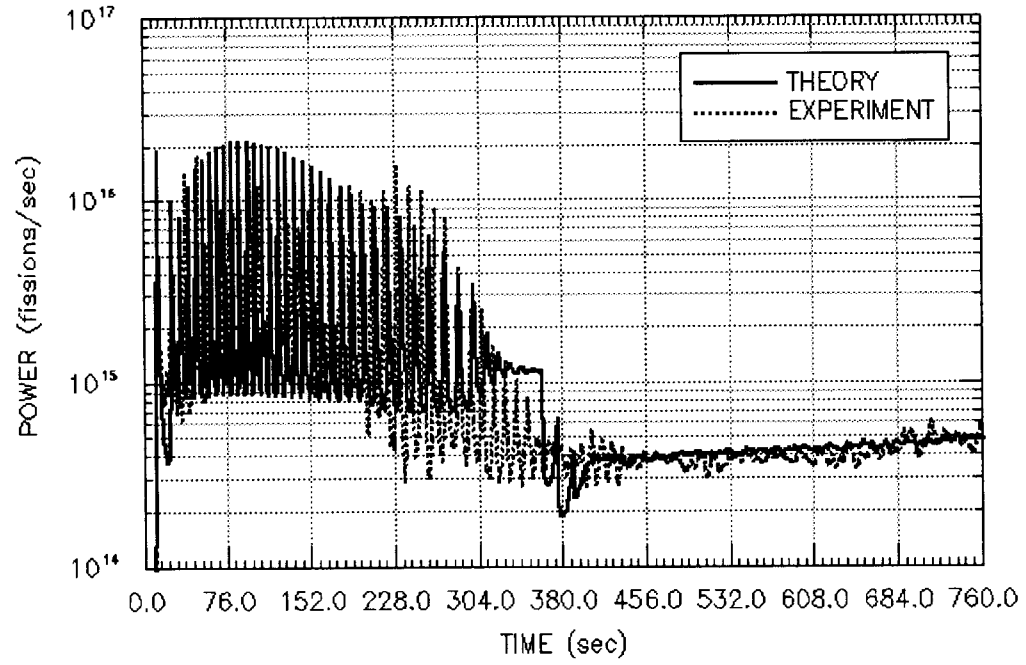

Fig. 5.6 Power versus Time: Comparison of TRACE Results with Experimental Results for CRAC 16

However, two main modeling difficulties (or weaknesses per say) may be observed from Fig. 5.6. First, even though TRACE can estimate the regions for power oscillations and the boiling plateau on the power curve very good, the transition between these two regions is not represented good enough. As can be seen in Fig. 5.6, there is a discontinuity in the TRACE calculated results. This discontinuity is as a result of treating boiling as a threshold phenomena. In reality, however, the transition is more continuous and the experimental power curve does not reveal any sharp discontinuity. Experimental results have shown that boiling process, in fact, is not a threshold phenomena, but it develops in a gradual manner. Thus further improvements should be made on the boiling model for the transition phase.

Second weakness in the modeling is due to the beat pattern in the power oscillations. Even though TRACE can estimate the general behavior of the power oscillations and gradual decrease in peak magnitude quite well, the beating nature of the power oscillations can not be estimated using the present model. This phenomenon also needs further attention in future studies.

In summary TRACE, at present, can not model the transition region between power oscillations and the boiling plateau. Moreover, TRACE is unable to consider beating nature of the power oscillations.

5.8. CRAC 18 Experiment

CRAC 18 experiment investigated a criticality transient involving 93% enriched uranyl nitrate solution with an uranium mass of 2.29 kg (2.13 kg of ^{235}U mass). The acidity and the NO_3^- molarity of the fissile liquid was 2.00 N and 2.68 N, respectively. CRAC 18 is performed to investigate the behavior of a long-duration, boiling type solution transients. The fissile system was initially at critical condition at a low steady state power when the ramp reactivity addition was initiated. Solution height at start of solution addition was 41.97 cm. Solution was added into the system at a rate of 104 liter/h (2.89×10^{-5} m^3/s). This addition resulted initially in a uniform ramp reactivity increase of 0.0168 \$/s. The reactivity addition continued 1404 seconds until the height reached 102.4 cm. The

experiment ended in approximately 360 minutes. The first fission pulse was observed 43.8 seconds after delayed criticality with a peak power of 7.7×10^{15} fissions/s.

This experiment is modeled using TRACE only for the first 300 seconds. TRACE, at present, can not model the gradual decrease in system power starting from approximately 300 seconds after criticality. This is most likely due to insufficient representation of the temperature reactivity feedback phenomenon by the Monte Carlo calculated feedback function.

In this experiment, the void velocity model is modified to obtain good agreement with the experiment. The void velocity is multiplied by a correction factor in the time interval between the spike and the second fission pulse. Physical meaning of this approach is given in Section 5.13.

TRACE can provide a satisfactory estimate for CRAC 18 by using a G-value of 1×10^{-7} mol/J and a θ-value of 3.5×10^{-7} m^3/J·mol for the radiolytic gas model. However, the shape and the peak power of the first fission pulse do not agree with the experiment. On the other hand, TRACE calculated results agrees well with the experiments, when the initial reactivity of the system is assumed to be 40 ¢ and the initiation time is set to be 40 seconds.

Figure 5.7 shows the computer simulation of CRAC 18 experiment for the first 300 seconds. The code predicts the first fission pulse as 5.45×10^{15} fissions/s where the time to the peak from delayed critical is estimated as 43.1 s. The new velocity model is employed in the simulation where the quantities v_{g0} and γ are assumed to 0.022 m/s and 0.02, respectively.

CRAC 18 is indeed a good candidate for evaluating the boiling model because it is a long-duration boiling-type experiment where the temperature of the fissile liquid rises above the boiling temperature. Therefore, CRAC 18 has to be considered in detail in future studies.

5.9. CRAC 20-4 Experiment

CRAC 20-4 experiment considers a criticality transient involving 93% enriched uranyl nitrate solution with an uranium mass of 4.09 kg (3.81 kg of ^{235}U mass). The fuel

concentration in CRAC 20-4 and CRAC 20-5 experiments was relatively high (218 g/liter). The acidity and the NO_3^- molarity of the fissile liquid was 2.32 N and 4.165 N, respectively.

Solution height at start of solution addition was 4.92 cm where the system was subcritical. Solution was added into the system at a rate of 1489 liter/h (4.14×10^{-4} m^3/s). This addition resulted initially in a uniform ramp reactivity increase of 0.685 \$/s. The system reached the critical height 27.1 cm in 36.2 s. Following criticality, solution addition continued 5.8 s until the height reached 30.6 cm. The first fission pulse was observed 3.36 seconds after delayed criticality with a peak power of 1.0×10^{19} fissions/s.

Figure 5.8 shows power with respect to time for CRAC 20-4 for the full time range of the reported experimental data. As can be seen in this figure, the agreement between the calculated and the experimental data is very good. The code predicts the first fission pulse as 1.06×10^{19} fissions/s. Moreover, time to the peak from delayed critical is estimated as 3.346 s. The new velocity model is employed in the simulation where the quantities v_{g0} and γ are assumed to 0.02 m/s and 0.01, respectively. Also, a G -value of 1.08×10^{-7} mol/J and a θ -value of 2×10^{-6} $m^3/J\cdot mol$ are used for the modeling of radiolytic gas phenomenon. TRACE estimates the total inherent neutron source strength of CRAC 20-4 as 342 neutrons/s. No initiation time is used for the modeling.

5.10. CRAC 20-5 Experiment

CRAC 20-5 experiment was conducted using the same experimental setup as CRAC 20-4. This experiment was done within 30 minutes after CRAC 20-4 experiment. Solution height at start of solution addition was 4.91 cm and the system was subcritical. Solution was added into the system at a rate of 1340 liter/h (3.72×10^{-4} m^3/s). This addition resulted initially in a uniform ramp reactivity increase of 0.616 \$/s. In this experiment, the system reached prompt critical condition in less than 2 seconds.

The system attained the critical height 27.10 cm in 40.3 seconds. Following criticality, solution addition continued 10.7 s until the height reached 33 cm. The first fission pulse was observed 2.53 seconds after delayed criticality and the transient resulted in a peak power of 5.8×10^{17} fissions/s.

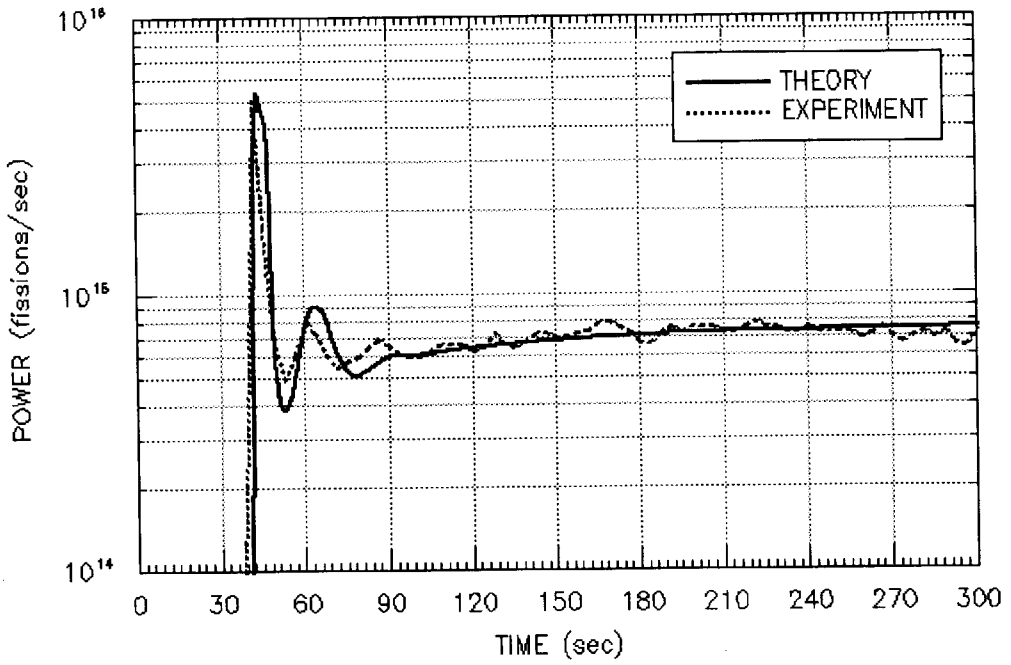

Fig. 5.7 Power versus Time: Comparison of TRACE Results with Experimental Results for CRAC 18

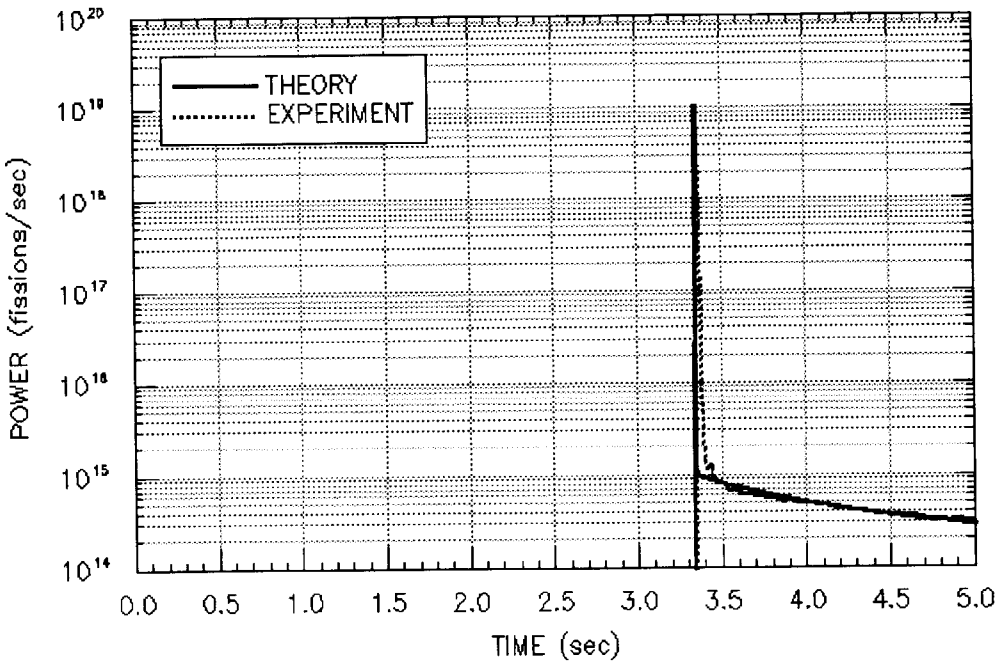

Fig. 5.8 Power versus Time: Comparison of TRACE Results with Experimental Results for CRAC 20-4

Figure 5.9 shows the computer simulation of CRAC 20-5 experiment for the first 100 seconds using a G-value of 1.466×10^{-8} mol/J and a θ-value of 1×10^{-8} m^3/J·mol for the radiolytic gas model. The code predicts the first fission pulse as 5.99×10^{17} fissions/s where the time to the peak from delayed critical is estimated as 1.9 s. CRITEX-type two velocity approach is used in the simulation since this approach produced a good agreement with the experimental results. The code, however, cannot predict the beating nature of the power oscillations. But TRACE can estimate the general behavior of the power curve quite good. No initiation time is used for the modeling.

5.11. CRAC 22 Experiment

CRAC 22 experiment was done using a 300-mm-diam vessel containing 93% enriched uranyl nitrate solution with an uranium mass of 3.86 kg (3.60 kg of ^{235}U mass). The acidity and the NO_3^- molarity of the fissile liquid was 2.07 N and 3.83 N, respectively. The experiment continued approximately 6 minutes. Solution height at start of solution addition was 7.9 cm where the system was subcritical. Solution was added into the system at a rate of 1066 liter/h (2.96×10^{-4} m^3/s). This initial uniform ramp reactivity increase was equal to 0.501 \$/s. The system reached the critical height 26.91 cm in 43.4 seconds. Following criticality, solution addition continued 14.6 s until height reached 33.3 cm. The first fission pulse was observed 4.57 seconds after delayed criticality with a peak power of 5.4×10^{18} fissions/s.

Figure 5.10 shows the computer simulation of CRAC 22 experiment for the first 15 seconds. As can be observed from this figure, there is an excellent agreement between TRACE and the experiment. The code predicts the first fission pulse as 2.28×10^{18} fissions/s where the time to the peak from delayed critical is estimated as 4.34 s. The quantities v_{g0} and γ for the new void velocity model are assumed to 0.022 m/s and 0.022, respectively. Also, a G-value of 8.424×10^{-8} mol/J and a θ-value of 3×10^{-6} m^3/J·mol are used for the modeling. Initiation time is equal to 4.3 s for this experiment. It is assumed that the initial power is small. TRACE estimates the total inherent neutron source strength of this experiment as 299 neutrons/s.

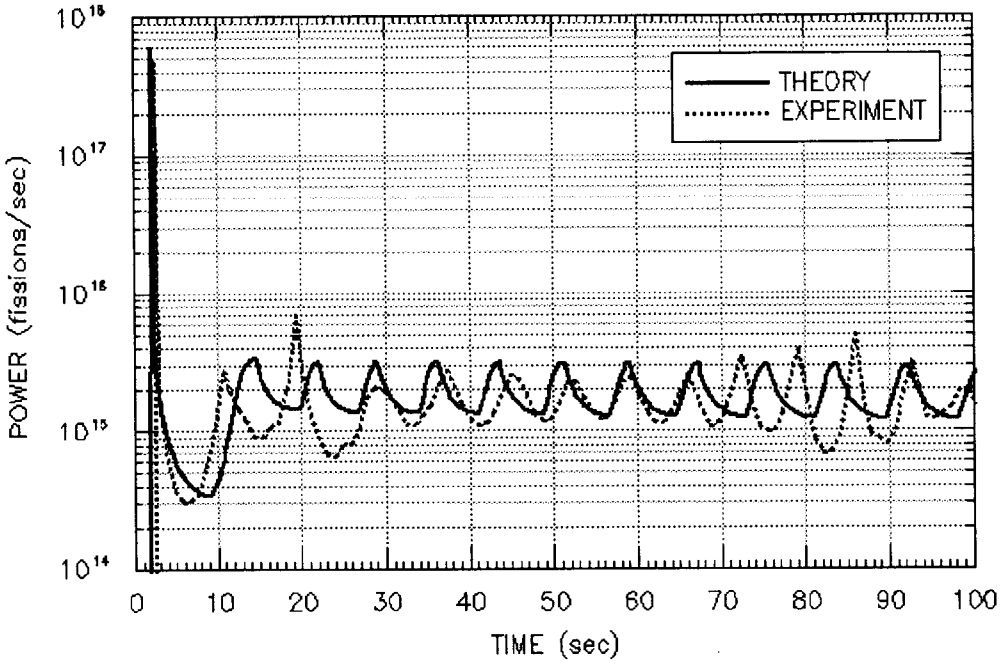

Fig. 5.9 Power versus Time: Comparison of TRACE Results with Experimental Results for CRAC 20-5

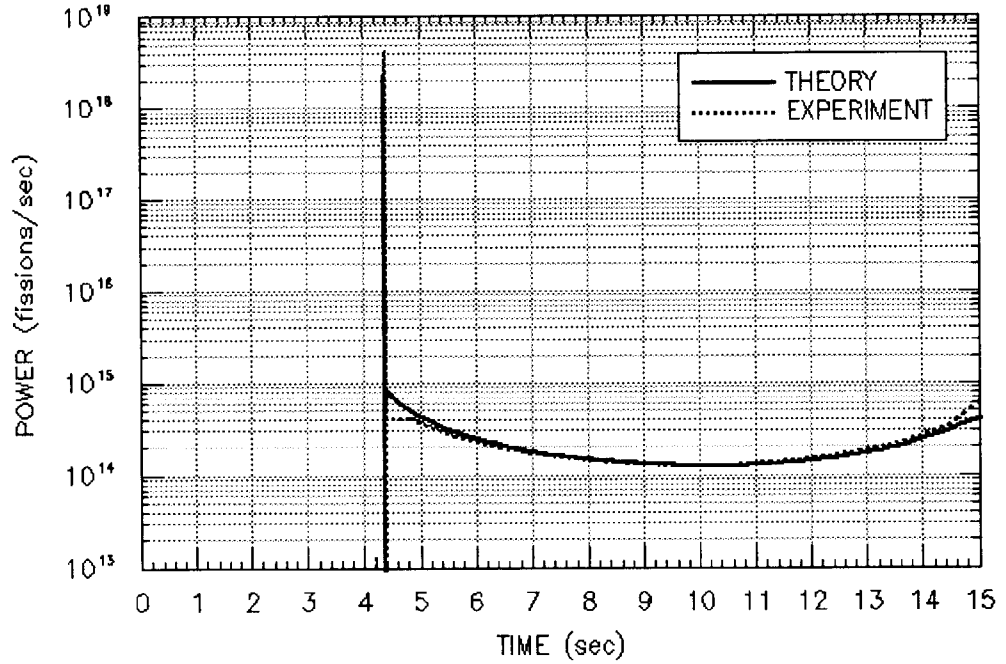

Fig. 5.10 Power versus Time: Comparison of TRACE Results with Experimental Results for CRAC 22

5.12. CRAC 37 Experiment

CRAC 37 experiment was conducted using 800-mm-diam vessel. The fuel was 93% enriched uranyl nitrate solution with an uranium mass of 4.84 kg (4.50 kg of ^{235}U mass). The acidity and the NO_3^- molarity of the fissile liquid was 2.00 N and 2.20 N, respectively. The fuel concentration for CRAC 37 was very low (21.8 g/liter)

The solution height at start of solution addition was 44 cm where the system was at subcritical condition. Solution was added into the system at a rate of 448 liter/h (1.24×10^{-4} m^3/s). This addition resulted initially in a uniform ramp reactivity increase of 0.00381 \$/s. The system reached the critical height 45 cm in 40 seconds. Following criticality, solution addition continued 282 seconds. The final solution height was 52.1 cm. The experiment continued approximately 6 minutes. The first fission pulse was observed 72.8 s after delayed criticality with a peak power of 8.6×10^{16} fissions/s.

Since the vessel was large in diameter, radial effects for thermal hydraulics are expected to be more important for this experiment. The spatial effects for neutronics may also be significant since large systems are more susceptible for local perturbations such as surface waves.

Moreover, it was noticed that CSAS25 sequence of SCALE is not appropriate for the estimation of the temperature feedback coefficient for CRAC 37. Because the fuel concentration is very low, the temperature feedback coefficient is expected to be small. As a result, the uncertainty in the Monte Carlo results can not be safety ignored since their magnitude is comparable with the reactivity differences for CRAC 37. It is expected that results are sensitive to the temperature feedback coefficient. Therefore, two different sets of calculations are conducted for CRAC 37. First set uses the CSAS25 estimated temperature reactivity feedback function by ignoring the Monte Carlo uncertainty. The second set uses a simple linear temperature feedback coefficient estimated by a parametric study. Figure 5.11 shows the results of both sets of calculations along with the experimental results. Agreement is excellent for the case where the temperature coefficient is calculated by a parametric study (i.e., the second set of calculations). The agreement for the other set may be considered satisfactory.

For the second set of calculations, the code predicts the first fission pulse as 1.36×10^{17} fissions/s where the time to the peak from delayed critical is estimated as 71.1 s. The new velocity model is employed in the simulation where the quantities v_{g0} and γ are assumed to 0.018 m/s and 0.009, respectively. Also, a G -value of 1.5×10^{-7} mol/J and a θ-value of 1×10^{-8} m^3/J·mol are used for the modeling of radiolytic gas phenomenon. No initiation time is used for CRAC 37. Also the initial power is assumed to very small. TRACE estimates the total inherent neutron source strength of this experiment as 463 neutrons/s.

Because of the reasons given above, CRAC 37 simulation results presented in this section should be used with caution. Future analysis for CRAC 37 needs to include spatial effects in the modeling. Moreover, future studies have to consider more careful evaluation of the temperature reactivity feedback coefficient of CRAC 37.

5.13. CRAC 50 Experiment

CRAC 50 experiment investigated a criticality transient involving 93% enriched uranyl nitrate solution with an uranium mass of 2.37 kg (2.21 kg of ^{235}U mass). The acidity and the NO_3^- molarity of the fissile liquid was 2.05 N and 2.74 N, respectively. Solution height at start of solution addition was 40.25 cm where the system was subcritical. Solution was added into the system at a rate of 511 liter/h (1.42×10^{-4} m^3/s). This addition resulted initially in a uniform ramp reactivity increase of 0.247 \$/s. The system reached the critical height 40.50 cm. Following criticality, solution addition continued 94 s until the height reached 63.2 cm. The experiment continued approximately 5 minutes. The first fission pulse was observed 15 seconds after delayed criticality with a peak power of 1.0×10^{17} fissions/s.

In this experiment, the void velocity model is modified to obtain good agreement with the experimental results. The void velocity is multiplied by a correction factor in the time interval between the spike and the second fission pulse. Physically this means that the radiolytic gas production rate is large due to the high size of spike (which one order of magnitude larger then the succeeding pulses for CRAC 50). As a result, the gas bubbles can have a larger size and can move upwards with a faster velocity due to buoyant forces

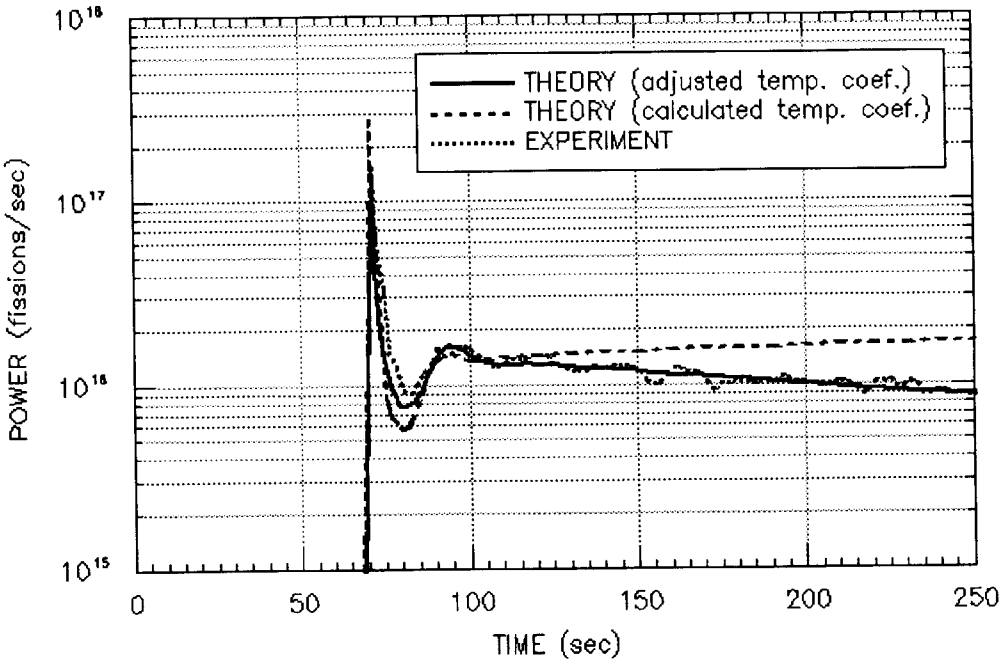

Fig. 5.11 Power versus Time: Comparison of TRACE Results with Experimental Results for CRAC 37

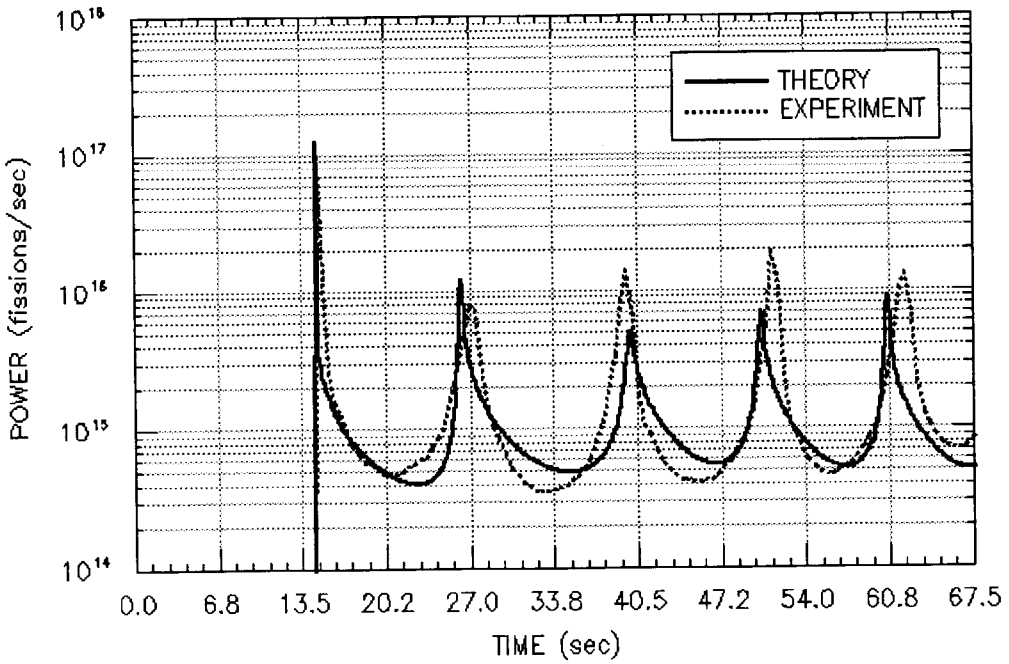

Fig. 5.12 Power versus Time: Comparison of TRACE Results with Experimental Results for CRAC 50

acting on them. This correction factor is equal to 1.5 for CRAC 50. This approach, then, gives good agreement between the TRACE calculated results and the experimental results as shown in Fig. 5.12. This figure provides the power history of CRAC 50 experiment for the first 5 fission pulses. The code predicts the first fission pulse as 1.25×10^{17} fissions/s where the time to the peak from delayed critical is estimated as 14.6 s. The quantities v_{g0} and γ for the new void velocity model are assumed to be 0.012 m/s and 0.062, respectively. Also, a C_j-value of 7×10^{-7} mol/J and a ϑ-value of 4×10^{-8} m^3/J·mol are used for the modeling of radiolytic gas phenomenon. The initiation time is assumed to be 14.3 s. The initial power is assumed to be small. TRACE estimates the total inherent neutron source strength of this experiment as 200 neutrons/s.

5.14. CRAC 52 Experiment

CRAC 52 experiment investigated a criticality transient involving 93% enriched uranyl nitrate solution with an uranium mass of 2.37 kg (2.21 kg of ^{235}U mass). The acidity of the fissile liquid was 2.18 N. Solution height at start of solution addition was 39.41 cm where the system was subcritical. Solution was added into the system at a rate of 552 liter/h (1.53×10^{-4} m^3/s). This addition resulted initially in a uniform ramp reactivity increase of 0.247 \$/s. The system reached the critical height 40.41 cm. Following criticality, solution addition continued 98 s until the height reached 64.8 cm. The first fission pulse was observed 7.9 seconds after delayed criticality with a peak power of 4.2×10^{17} fissions/s.

Figure 5.13 shows the computer simulation of CRAC 52 experiment for the first 5 fission pulses. The new void velocity model is employed in the simulation where the quantities v_{g0} and γ are assumed to 0.014 m/s and 0.08, respectively.

For CRAC 52, the size of the spike is approximately two orders of magnitude larger than the succeeding fission pulses. Hence, the void velocity is also multiplied by a correction factor (which is equal to 1.5) for this experiment as in CRAC 50 for the time interval between the spike and the second fission pulse. Moreover, TRACE calculated results for the large size of the first fission pulse agree well with the experiments as shown in Fig. 5.13, when the initiation time is set to be 7.2 seconds and the initial reactivity of the

system is taken to be 40 ¢. Also, a G-value of 3×10^{-7} mol/J and a θ-value of 1×10^{-7} m^3/J·mol are used for TRACE results shown in Fig. 5.13. The code predicts the first fission pulse as 2.84×10^{17} fissions/s where the time to the peak from delayed critical is estimated as 7.5 s. TRACE calculates the total inherent neutron source strength of this experiment as 207 neutrons/s.

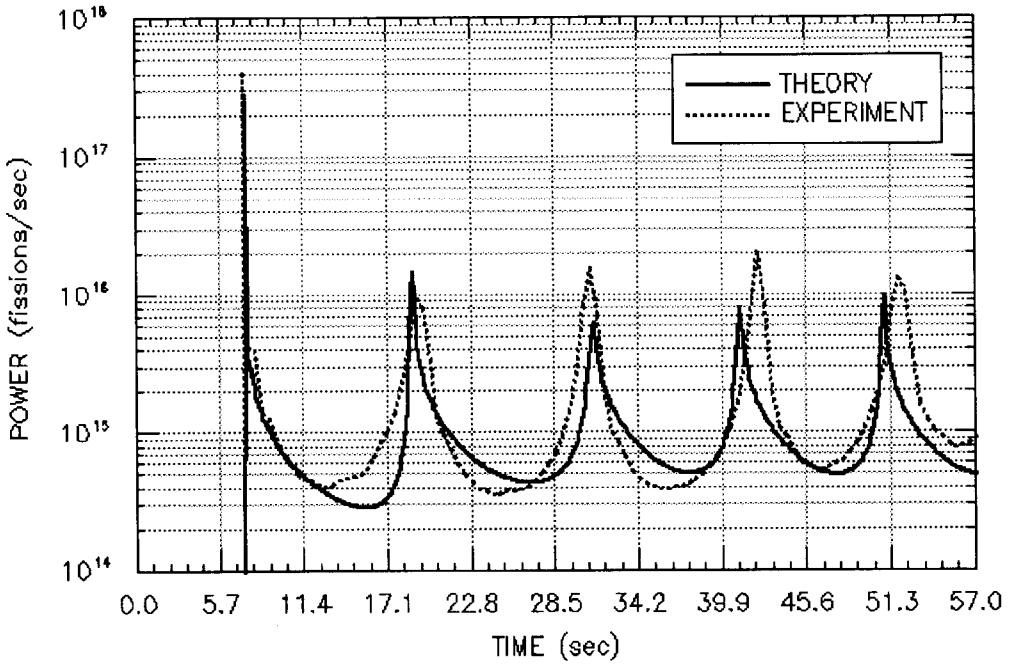

Fig. 5.13 Power versus Time: Comparison of TRACE Results with Experimental Results for CRAC 52

6. CONCLUSIONS

The TRACE code has been developed in order to model criticality transients involving fissile solutions of uranium and plutonium. This research should be viewed as one of the first attempts at modeling boiling phenomena of criticality excursions of fissile liquids. The results presented in this report are for several CRAC experiments which are calculated using the new simulation code.

The excursion studies presented in this work permit several conclusions to be drawn about the TRACE code. First, simulation results presented in this report have shown that TRACE can produce satisfactory estimates for fissile liquid transients including the general behavior of the boiling systems. However, the thermal-hydraulic and neutronics modeling is still far from complete. There are many areas for future improvement. Boiling model used in TRACE is very simple and can further be improved. For instance, TRACE can not model the transition region from non-boiling phase to boiling phase. The code treats boiling as a threshold phenomena. Experiments, however, have shown that boiling develops in a gradual manner. Second, TRACE can not model beating nature of the power oscillations. This phenomenon also needs further attention in future studies.

Moreover, space-dependent effects may be important for some systems and provisions have to be made to include space-dependent phenomena for the neutronic modeling. Future studies also need to consider more careful evaluation of the reactivity feedback functions.

New models should be incorporated into the code to reduce the number of tune-up parameters. Functional dependence of some void model related parameters (which are assumed to be constant in this work) should be investigated in more detail.

Finally, new experiments should be performed on excursion characteristics as well as thermal hydraulic behavior of fissile solutions.

REFERENCES

1. STRATTON, W.R. :"A Review of Criticality Accidents", DOE/NTC-04 (1989).

2. DUNENFELD, M.S., STITT, R.K. :"Summary of the Kinetics Experiments on Water Boilers", Atomics International, NAA-SR-7087 (1963).

3. NEWLON, C.E., HANSEN, A.N., FITHIAN, C. :"An Assessment of the Minimum Criticality Accident of Concern", H&R 82-2, H&R Technical Associates Inc., Oak Ridge, Tennessee (1982).

4. LECORCHE, P., SEALE, R.L. :"A Review of the Experiments Performed to Determine the Radiological Consequences of a Criticality Accident", Y-CDC-12, Oak Ridge Y-12 Plant (1973).

5. BARBRY, F. : "Fuel Solution Criticality Accident Studies with the SILENE Reactor", *Proc. Int. Seminar Criticality Studies Program and Needs*, Dijon, France September 19-22, 1983.

6. NAKAJIMA, K. et al. :"Experimental Study on Criticality Accidents Using TRACY", *Conference on the Physics of Reactors*, 4, L•83-92, Mito, Ibaraki, Japan, September 16-20, 1996.

7. HETRICK, D.L. :"Simulation of Power Pulses in Criticality Accidents with Fissile Solutions", *Proceedings of the International Topical Meeting on Safety Margins in Criticality Safety*, San Francisco, California, U.S.A., November 26-30, 1989.

8. MATHER, D.J., SHAW, P.M. :"CRITEX - A Computer Program to Calculate Criticality Excursions in Fissile Liquid Systems", SRD R 380, UK Atomic Energy Authority (July 1984).

9. KATO, R. et al. :"The Code CREST to Simulate Criticality Excursion in Fuel Solution", *Proceedings of the International Topical Meeting on Safety Margins in Criticality Safety*, San Francisco, California, U.S.A., November 26-30, 1989.

10. BREWER, R.W. :"Analysis of a Hypothetical Array Criticality Accident Involving Units of Aqueous Uranyl Fluoride", M.S. Thesis, The University of Tennessee, Knoxville (1993).

11. NAKAJIMA, K., YANAGISAWA, H. :"Development of a Kinetics Code, AGNES, for the Evaluation of Criticality Accidents in Solution Fuel Systems", *International Seminar on Nuclear Criticality Safety*, Tokyo, Japan, October 19-23, 1987.

12. NAKAJIMA, K., OHNISHI, N. : "Development of AGNES, A Kinetics Code for Fissile Solutions (Part 1: Calculation of the Radiolytic Gas Void by Pressure Model)", Japan Atomic Energy Research Institute, JAERI-M 85-212 (1986).

13. MATHER, D.J. :"Analysis of Radiolytic Gas Nucleation During Criticality Transients", *Proceedings of the Fifth International Conference on Nuclear Criticality Safety*, Albuquerque, New Mexico, U.S.A., 2, 10•11-18, September 17-21, 1995.

14. LEWINS, J. :"Nuclear Reactor Kinetics and Control", Pergamon Press, Oxford (1978).

15. ASH, M. :"Nuclear Reactor Kinetics", McGraw-Hill Inc., New York (1979).

16. BASOGLU, B. :"Analysis of a Hypothetical Criticality Accident Involving Damp Low Enriched UO_2 Powder", M.S. Thesis, The University of Tennessee, Knoxville (1992).

17. "SCALE: A Modular Code System for Performing Standardized Computer Analyses for Licensing Evaluation," NUREG/CR-0200, 1-5 (1990).

18. PETRIE, L.M., LANDERS, N.F. :"KENO V.a: An improved Monte Carlo Criticality Program with Supergrouping", NUREG/CR-0200, 2, ORNL/NUREG/CSD-2/R5 (September 1995).

19. HANSEN, G.E. :"Assembly of Fissionable Material in the Presence of a Weak Neutron Source", *Nucl. Sci. and Eng.*, 8, 709 (1990).

20. LLOYD, R.C. et al. :"Criticality Studies with Plutonium Solutions", *Nucl. Sci. and Eng.*, 25, 165 (1966).

21. MATSUNOBU, H. :"Data Book for Calculating Neutron Yields from (α,n) Reaction and Spontaneous Fission", Japan Atomic Energy Research Institute, JAERI-1324 (1992).

22. HANKINS, D.E. :"Effect of Reactivity Addition Rate and of Weak Neutron Source on the Fission Yield of Uranium Solutions", *Nucl. Sci. and Eng.*, 26, 110 (1966).

23. SEALE, R.L., ANDERSON, R.E. :"Intrinsic Neutron Source Strengths in Uranium Solutions", *Trans. Am. Nucl. Soc.*, 63, 226 (1991).

24. MEE, W.T. :"Consequences of a Postulated, Moderated Criticality Accident at the Oak Ridge Y-12 Plant", Y/DD-384, Oak Ridge Y-12 Plant, Oak Ridge, Tennessee (1988).

25. LUTZ, H.F. :"Nuclear Criticality Safety Assessment Calculations: Part I. Calculating Power Histories in Nuclear Excursions", H.J. KROOPNICK, Ed., M-164, Lawrence Livermore National Lab., Livermore, California (1985).

26. WHITAKER, S. :"Fundamental Principles of Heat Transfer", Pergamon Press Inc., New York (1977).

27. CROFT, D.R., LILLEY, D.G. :"Heat Transfer Calculations Using Finite Difference Equations", Applied Science Publishers Ltd., London (1977).

28. SCHULENBERG, T., DOHLER, J. :"Heating-up, Nucleation and Boiling of a Critical Solution of Fissile Material", *Int. J. Multiphase Flow*, 12, 759 (1986).

29. CHOPPIN, G.R., RYDBERG, J. :"Nuclear Chemistry Theory and Applications", Pergamon Press, Oxford.

30. O'DONNELL, J.H., SANGSTER, D.F. :"Principles of Radiation Chemistry", Edward Arnold Publishers Ltd., London.

31. BIDWELL, R.M. et al. :"Radiolytic Yields of Nitrogen and Hydrogen in Water Boilers", *Nucl. Sci. and Eng.*, 1, 452 (1956).

32. SPIEGLER, P. et al. :"Production of Void and Pressure by Fission Track Nucleation of Radiolytic Gas Bubbles During Power Bursts in a Solution Reactor", Atomics International, NAA-SR-7086 (1962).

33. GLASSTONE, S. :"Textbook of Physical Chemistry", D. Van Nostrand Company Inc., New York (1946).

34. BATTINO, R., CLEVER, H.L. :"The Solubility of Gases in Liquids", *Chemical Reviews*, 66 (1966).

35. WARK, K. :"Thermodynamics", McGraw-Hill Inc., New York (1983).

36. SKINNER, R.E., HETRICK, D.L. :"The Transfer Function of a Water Boiler Reactor", *Nucl. Sci. and Eng.*, 3, 573 (1958).

37. HETSRONI, G. Ed. :"Handbook of Multiphase Systems", Hemisphere Publishing Corporation (1982).

38. VAN STRALEN, S., COLE, R. :"Boiling Phenomena: Physicochemical and Engineering Fundamentals and Applications", 1 and 2, Hemisphere Publishing Corporation (1979).

39. CHEREMISINOFF, N.P. Ed. :"Handbook of Heat and Mass Transfer, Volume 1: Heat Transfer Operations", Gulf Publishing Company (1986).

40. HAHNE, E., GRIGULL, U. :"Heat Transfer in Boiling", Hemisphere Publishing Corporation, Washington (1977).

41. FORSTER, H.K., ZUBER, N. :"Growth of a Vapor Bubble in a Superheated Liquid", *J. App. Phy.*, 25 (1954).

42. HSU, Y.Y., GRAHAM, R.W. :"Transport Processes in Boiling and Two-Phase Systems Including Near-Critical Fluids", Hemisphere Publishing Corporation (1976).

43. MCFADDEN, P.W., GRASSMAN, P. :"The Relationship Between Bubble Frequency and Diameter During Nucleate Pool Boiling", *Int. J. Heat Mass Transfer*, 5, 169 (1962).

44. Orth, E.W. et al. :"Hydrodynamic aspects of volumetric boiling", *Trans. Am. Nucl. Soc.*, 33, 545 (1979)

45. NOMURA, Y. :"Comparative Evaluation by STAR Code with Source Term Models used in Solution Heating and Boiling for Reprocessing Facility", Japan Atomic Energy Research Institute, JAERI-M 91-091 (1991).

46. POWERS, D.A. et al. :"VANESA, A Mechanical Model of Radionuclide Release and Aerosol Generation During Core Debris Interactions with Concrete", NUREG/CR-4308, SAND85-1370 (1986).

47. GINSBERG, T. :"Aerosol Generation by Liquid Breakup Resulting from Sparging of Molten Pools of Corium by Gases Released During Core/Concrete Interactions", *Nucl. Sci. and Eng.*, 89, 36 (1985).

48. HINDMARSH, A.C. :"LSODE and LSODI - Two New Initial Value Ordinary Differential Equation Solvers", *ACM-Signum Newsletter*, 15 (1980).

49. LAMBERT, J.D. :"Computational Methods in Ordinary Differential Equations", John Wiley and Sons, New York (1986).

50. KOBAYASHI, K. :"SPADE: a computer subroutine for generating steam tables having pressure and density as the independent variables", Japan Atomic Energy Research Institute, JAERI-M-7961 (1978)

51. TRACY Working Group, "Summary of the CRAC Experimental Conditions and Data," Japan Atomic Energy Research Institute, JAERI-M 89-031 (1989).

52. Nakajima, K. : private communication.

APPENDIX
TRACE USER'S MANUAL

A.1. Introduction

TRACE code uses four different input files, namely, TRACE.INP, TRACE.DBA, TRACE.EXP, and TRACE.KAN. TRACE.INP is the general input file. The input parameters for TRACE.INP are described in Section A.3. TRACE.DBA is an experimental database for the general input. It contains the input parameters, **diamin**, **diamou**, **theig**, **heig**, **confl**, **zmhy**, **zmno**, **zm24**, **zm25**, **zm28**, **zm49**, **zm40**, **igflg**, **amat**, **sca**, **xcmsl**, **war**, and **trend**, for several fissile solution excursion experiments which were conducted in the past. If TRACE.DBA database contains the information on the experiment under consideration, user can omit the above listed input parameters while setting up the TRACE.INP file. TRACE will automatically locate and read these parameters from TRACE.DBA.

TRACE also utilizes the TRACE.EXP file to plot experimental results on the screen. TRACE.EXP is an experimental database containing power, fission yield, reactivity, pressure, and temperature versus time results of several fissile criticality experiments. TRACE code automatically searches the solution title and plot parameter in TRACE.EXP file. If the experimental data are available, TRACE plots them on the screen for comparison with the theoretical results that are being calculated. At presents, TRACE.DBA and TRACE.EXP database files contain predominantly information on CRAC experiments.

Moreover, TRACE reads data for plotting KANJI characters from the TRACE.KAN file.

The TRACE calculated results are written into eleven different output files. The output files and their contents are summarized in Table A.1.

Table A.1

Contents of Output Files

FILENAME	CONTENTS
TRACE.POW	◆ Feedback reactivity (for void, temperature, concentration) versus time. ◆ External reactivity versus time. ◆ Total reactivity versus time. ◆ Inverse period versus time. ◆ Power and fission yield versus time.
TRACE.PRE	Liquid and gas pressures versus time.
TRACE.TEM	Temperature (full distribution or on a selected sensor location) versus time.
TRACE.VGM	Number of moles of radioytic gas versus time for each axial region.
TRACE.VGV	◆ Void volume of gas bubbles versus time for each axial region. ◆ Total void volume of gas bubbles versus time.
TRACE.ISS	Results of inherent neutron source strength calculations.
TRACE.MOT	Volume versus time (i.e., the fluid motion calculations).
TRACE.AER	Results of aerosol production calculations.
TRACE.BOI	◆ Void volume of vapor bubbles versus time for each region. ◆ Total void volume of vapor bubbles versus time.
TRACE.ERR	Error message, if program is terminated due to an error.
TRACE.WAR	Warning message(s).

A.2. Input Description

Namelist input format is used for the general input. Table A.2 shows a sample input file for TRACE. Each input parameter can be described as follows:

Namelist GENERAL

title - Title for the run (name of the experiment while modeling an experiment).

amat - Identification name of the fissile solution:

=uni : Uranyl nitrate.

=pni : Plutonium nitrate.

=ufl : Uranyl fluoride

amcn - Material name for the vessel:

=sst : Stainless Steel.

war - Rate of solution addition (kg/s or m^3/s).

Namelist LSODE

itol - Indicator for the type of error control:

=1 : **rtol** and **atol** are both scalars.

=2 : **rtol** is a scalar, **atol** is an array.

=3 : **rtol** is an array, **atol** is a scalar.

=4 : **rtol** and **atol** are both arrays.

rtol - Relative error tolerance parameter (scalar or an array of length **neq**).

atol - Absolute error tolerance parameter (scalar or an array of length **neq**).

itask - Index specifying the task to be performed:

=1 : For normal computation.

istate - Index used for input and output to specify the state of calculations.

=1 : First call for the problem.

iopt - Integer flag to specify whether or not any optional inputs are being used:

=0 : To indicate no optional input used.

lrw - User-declared length of real work array:

=20+16×**neq** : For **mf**=10.

=22+9×**neq**+**neq**^{2} : For **mf**=22.

liw - User-declared length of integer work array:

=20 : For **mf**=10,

=20+**neq** : For **mf**=22.

mf - Method flag:

=10 : For nonstiff (implicit-adams) method, no jacobian used.

=22 : For stiff (backward differentiation formula) method, internally generated full jacobian.

Namelist TIMING

tend - Final time location where the output is desired (i.e., time for end of run).

tinit - Initiation time for the first persistent chain reaction (weak neutron source considerations).

tinc - Length of each edit time interval.

trend - Time at which ramp reactivity addition is terminated.

Namelist GEOMETRIC

igflg - Vessel type flag:

=1 : CRAC 300-mm-diam type cylindrical vessel.

=2 : CRAC 800-mm-diam type cylindrical vessel.

=3 : TRACY type annular vessel.

nnradf - Number of radial regions.

nnaxif - Number of axial regions.

diamin - Inner diameter of the vessel.

diamou - Outer diameter of the vessel.

heig - Initial height of the fissile solution.

Namelist NEUTRONIC

irflg - External reactivity addition flag:

=1 : Volume addition. Linear feedback with respect to change in buckling.

=2 : Mass addition. Linear feedback with respect to change in buckling.

=3 : Quadratic formula.

=4 : Volume addition. 7^{th} order polynomial with respect to height of the fissile liquid.

=5 : Transient rod withdrawal (Step reactivity input).

ifflg - Temperature feedback reactivity flag:

=1 : Simple feedback.

=2 : Power weighted feedback.

=3 : Power-square weighted feedback.

ieflg - Void feedback reactivity flag:

=1 : Simple feedback.

=2 : Power weighted feedback.

=3 : Power-square weighted feedback.

amda(i) - Array of decay constants for delayed neutron precursors (**i**=1,2,...,6).

beta(i) - Array of fractions for delayed neutron precursors (**i**=1,2,...,6).

gen - Neutron mean generation time.

sour - Extraneous source neutron generation rate.

rhotmp$_i$ - Coefficients for temperature reactivity feedback function (**i**=1 and 2).

rhovoi$_i$ - Coefficients for void reactivity feedback function (**i**=1,2,...,7).

rhoext$_i$ - Coefficients for external reactivity driving force function (**i**=0,1,2,...,7)

rhocon$_i$ - Coefficients for fuel concentration reactivity feedback function (**i**=1 and 2).

pd0 - Initial power.

srp - Stable period.

bcoef - Change in system reactivity with respect to change in buckling.

zext - Axial extrapolation distance.

zlife - Neutron mean lifetime.

Namelist RADGAS

ivgflg - Gas bubble velocity model flag:

= 1 : Constant from input.

= 2 : Two different constants from input (CRITEX approach).

= 3 : New velocity model.

= 4 : Kihoh model.

= 5 : Rise velocity of bubble in an infinite pool of liquid.

= 6 : Winston model.

= 7 : Toshiba model.

= 8 : Viecenz-mayinger model.

= 9 : Kurbatov model.

=10 : Sterman model.

=11 : Peebles and Garber model.

=12 : Harmathy model.

icflg - Flag for threshold for the production of radiolytic gas bubbles:

= 1 : Calculate the threshold for the production of radiolytic gas bubbles for each axial region separately.

= 2 : Calculate the threshold for the production of radiolytic gas bubbles globally.

vel1 - Void velocity for **ivgflg**=1.

Void velocity when power is increasing for **ivgflg**=2.

Void velocity corresponding to ω =0 for **ivgflg**=3.

vdgsk - Void velocity when power is decreasing for **ivgflg**=2.
Void velocity tuning parameter for **ivgflg**=3.

velup - Upper limit of void velocity for **ivgflg**=3.

veldw - Lower limit of void velocity for **ivgflg**=3.

gvalue - Produced number of moles of radiolytic gas per unit energy.

satc - Critical value for the number of moles of the radiolytic gas.
= 0 : Use the empirical formula (from AGNES studies).
< 0 : Use the balance equation for the equilibrium radius and the Henry's Law.

$\mathbf{a_i}$ - Constants for the energy to void conversion factor (**i**=0,1 and 2)

$\mathbf{b_i}$ - Constants for the bubble model (**i**=0,1,2 and 4)

hmol - Mixing coefficient for the equalization of the amount of gas in solution over all the axial regions.

rgbura - Equilibrium radius of gas bubbles.

ioflg - Flag for the equalization of the amount of gas in solution over all regions:
= 0 : Do not equalize.
= 1 : Always equalize.
= 2 : Equalize when the power is decreasing.
= 3 : Equalize when the power is increasing.
= 4 : Equalize at the power minima.
= 5 : Equalize at the power maxima.

Namelist THERMAL

idflg - Bottom container wall heat transfer flag:
= 1 : Do not consider heat loss from the bottom container wall.
= 2 : Consider heat loss from the bottom container wall.

ivar - Flag for the utilization of the property data.
= 0 : water; subcooled, superheated.

= 1 : water; saturated steam by temperature.

= 2 : water; saturated steam by pressure.

= 3 : water; saturated liquid by temperature.

= 4 : water; saturated liquid by pressure.

= 5 : **imat**; atmospheric.

= 6 : water; atmospheric.

= 7 : **imat**; material specific.

hitc - Temperature mixing coefficient.

tinf - Ambient temperature.

xy - Initial temperature of the fissile liquid.

ithermo - Identification number of the radial region for locating the temperature sensor.

jthermo - Identification number of the axial region for locating the temperature sensor.

imflg - Temperature output flag:

= 0 : Output temperature results for the region where the temperature sensor is located according to values of **ithermo** and **jthermo**.

= 1 : Output full temperature distribution.

Namelist BOILING

iyflg - Flag for the equilibrium radius calculations:

= 1 : Assume $(h_{lv} / v_{lv} T)$ =constant and $T = T_{sat}$.

= 2 : Assume (h_{lv} / v_{lv}) =constant.

= 3 : Assume $v_{lv} = v_v = (R_g T / p_l)$.

= 4 : Assume $(2\sigma / p_l r_{eq}) << 1$.

= 5 : Empirical correlation.

= 6 : Equilibrium equation with inert gas present.

ikflg - Surface evaporation flag:

= 0 : Do not consider surface evaporation.

= 1 : Consider surface evaporation if the temperature of the fissile solution is greater than the saturation temperature.

= 2 : Consider surface evaporation at all temperatures.

ilflg - Boiling simulation flag:

= 0 : Do not consider boiling.

= 1 : Estimate bubble departure radius for water using an empirical correlation.

= 2 : Estimate bubble departure radius for liquids other than water using an empirical correlation.

= 3 : Estimate bubble departure radius by simple force balance.

ivsflg - Vapor bubble velocity model flag (same options as **ivgflg**).

isflg - Total regional void volume flag:

= 0 : Radiolytic gas and vapor do not share the same volume.

= 1 : Radiolytic gas and vapor share the same volume.

radeq - Critical radius for the onset of boiling.

cbc_i - Empirical constants for the bubble population density calculations (**i**=1,2,3, and 4).

pga - Initial radiolytic gas pressure.

afreq - Constant for the waiting period calculations (i.e., the boiling simulation).

< 0 : Assume that waiting period is equal to zero.

svel1 - Vapor bubble velocity for **ivsflg**=1.

Vapor bubble velocity when power is increasing for **ivsflg**=2.

Vapor bubble velocity corresponding to ω =0 for **ivsflg**=3.

svdgsk - Vapor bubble velocity when power is decreasing for **ivsflg**=2.

Vapor bubble velocity tuning parameter for **ivgflg**=3.

evcoef - Correction factor for the surface evaporation calculations.

stbura - Radius of vapor bubbles.

Namelist MOTION

izflg - Fluid motion flag:
= 0 : Do not perform fluid motion calculations.
= 1 : Assume zero liquid pressure for faster reassembly.
= 2 : Assume atmospheric liquid pressure for slower reassembly.

discof - Empirical constant to account for momentum dissipation.

expcof - Constant for exponential pressure decay.

Namelist PLOT

ipflg - Vessel plot type flag:
= 1 : CRAC 300-mm-diam type cylindrical vessel.
= 2 : CRAC 800-mm-diam type cylindrical vessel.
= 3 : TRACY type annular vessel.

xmin - Lower limit of the y-axis for the power (total fissions, temperature, or pressure) plot.

xmax - Upper limit of the y-axis for the power (total fissions, temperature, or pressure) plot.

voimin - Lower limit of the void volume for the gray-scale-coded void volume indicator.

voima - Upper limit of the void volume for the gray-scale-coded void volume indicator.

reamin - Lower limit of the y-axis for the reactivity plots.

reamax - Upper limit of the y-axis for the reactivity plots.

tdelta - Temperature increment for the color-coded temperature distribution indicator.

tdelst - Initial temperature for the color-coded temperature distribution indicator.

sca - Global scaling parameter for graphical interface.

theig - Height of the vessel.

xcmsl - Frequency of the tic marks on the ruler indicating the height of the solution.

pdata - Plot flag:

= pow : Plot power versus time.

= fis : Plot total fissions versus time.

= tem : Plot temperature versus time.

= pre : Plot pressure versus time.

iouti - Output frequency (i.e., number of time steps between printouts/graphics screen updates).

Namelist COUNTER

icrtra - = 0 : Do not count the fission pulses.

= 1 : Count the fission pulses.

icrit - Sensitivity constant for counting the fission pulses.

Namelist PRESSURE

itflg - Pressure model flag:

= 0 : Simple model.

= 1 : Semi-empirical formula based on KEWB experiments.

= 2 : One-dimensional hydrodynamics equations.

zcons - Conversion constant for **itflg**=1 (=2.9×10^{-5} recommended).

pbias - Pressure bias for **itflg**=1.

prp - Pressure relaxation period for **itflg**=1.

gh2 - G-value of H_2 gas for **itflg**=1.

prcons - Correction factor for the alteration of the speed of sound for **itflg**=2

(=2×10^{-8} recommended).

Namelist AERO

inflg - Flag for aerosol generation calculations:

= 0 : Do not conduct aerosol generation calculations.

= 1 : Conduct aerosol generation calculations.

ihflg - Model for terminal bubble velocity calculations.

= 1 : Peebles and Garber model.

= 2 : Harmathy model.

iaflg - Film cap geometry estimate flag.

= 1 : Upper limit.

= 2 : Cipriano and Blanchard.

= 3 : Garner et al. (single bubble experiments).

= 4 : Garner et al. (with impurities).

= 5 : Azbel entrainment model.

= 6 : Tomaides and Whitby.

= 7 : German PSE (Projekt Sirherheit Endsorgung) model.

xperc - Constant for the film cap geometry estimate for **iaflg**=3 and **iaflg**=4.

fde - Fraction of droplets ejected with a radius greater than a given value.

fcth - Film cap thickness at the instant of bubble burst.

hdist1 - Distance from the free liquid surface (aerosol generation calculations for the deposition controlled region).

Namelist SOURCE

ibflg - Flag for inherent neutron source strength calculations.

= 1 : Use experimental results.

= 2 : Calculate the inherent neutron source strength.

zm24 - Weight percent of ^{234}U for uranium solutions.

zm25 - Weight percent of ^{235}U for uranium solutions.

zm28 - Weight percent of ^{238}U for uranium solutions.

zm49 - Weight percent of ^{239}Pu for plutonium solutions.

zm40 - Weight percent of ^{240}Pu for plutonium solutions.

zmhy - Acid Molarity.

zmno - Molarity of NO_3^-.

A.3. Description of Subroutines

The purpose of each subprogram is briefly described in the following list.

trace - This routine is the main program. It calls several routines to perform the following tasks:

- Open I/O files,
- Read input and library data,
- Perform initialization, and
- Calculate inherent neutron source strength.

This program also controls the primary flow of calculations.

aerosol - This subroutine controls the flow of aerosol production calculations.

prsspul - This subroutine is responsible for running the pressure model to calculate the pressure of the center of mass.

surfevap - This subroutine is called by **trace** to calculate the heat and mass loss rates due to surface evaporation.

boiling - This subroutine controls the boiling calculations.

fpass - This subroutine is called to update the reactivity information.

f - This subroutine is required by LSODE. It contains differential equation

for point neutronics. It also calls several subprograms to solve differential equations for the gas/vapor void motion, the heat transfer, and the fluid motion.

gasbulk - This subroutine is responsible for modeling the void effects for the bubbles generated due to mechanical pressure difference driven mechanism. It contains differential equations for the gas bulk model.

steambulk - This subroutine is responsible for modeling the movement of vapor bubbles after departure. It contains differential equations for the vapor bulk model.

eqofmo - This subroutine is called to solve the simple equation of motion. It contains a differential equation to estimate the acceleration of the center of mass.

tdc1d - This subroutine is responsible for conducting one-dimensional heat transfer calculations for a cylindrical vessel. It sets up differential equations to estimate temperature profiles for each radial region.

tdc2d - This subroutine is responsible for conducting two-dimensional (radial and axial) heat transfer calculations for a cylindrical vessel. It sets up differential equations to estimate temperature profiles for each region.

modmix - This subroutine averages the amount of gas in solution over all the regions using a mixing coefficient.

extreac - This function calculates the external reactivity.

fdbtemp - This subroutine calculates the feedback reactivity due to change in temperature.

fdbconc - This subroutine calculates the feedback reactivity due to change in fuel concentration.

fdbvoid - This subroutine calculates the feedback reactivity due to change in void volume.

vfdpar - This subroutine calculates the bubble model constant and the energy-to-void conversion factor.

plscount - This subroutine counts the power pulses.

geomup - This subroutine updates the geometrical variables at every edit time interval.

initgen - This subroutine conducts the initial calculations.

rdgen - This subroutine opens I/O files. It also reads the input and the library database files.

rhoinit - This subroutine initializes the coefficients of external and feedback reactivity functions.

wrout - This subroutine outputs the results at each output time interval.

boical - This subroutine controls the boiling simulation.

bubrad - This function calculates the bubble diameter.

magsup - This logical function calculates the magnitude of the superheat required for a given critical radius.

boiche - This subroutine checks if the boiling could start or not.

eqlrad - This function calculates the critical radius for a given superheat.

plicrac1 - This subroutine initializes the plot variables and windows for CRAC 300-mm-diam type cylindrical vessels. It plots the container walls and also calls necessary subroutines to plot the scaled ruler and the experimental data.

plicrac2 - This subroutine initializes the plot variables and windows for CRAC 800-mm-diam type cylindrical vessels. It plots the container walls and also calls necessary subroutines to plot the scaled ruler and the experimental data.

plitrac - This subroutine initializes the plot variables and windows for TRACY type annular vessels. It plots the container walls and also calls necessary subroutines to plot the scaled ruler and the experimental data.

pld1crac - This subroutine updates the graphics screen for CRAC 300-mm-diam type cylindrical vessels by calling the necessary subroutines as the program runs.

pld2crac - This subroutine updates the graphics screen for CRAC 800-mm-diam type cylindrical vessels by calling the necessary subroutines as the

program runs.

pldtrac - This subroutine updates the graphics screen for TRACY type annular vessels by calling the necessary subroutines as the program runs.

plupdat - This subroutine is called to update results (time, average temperature, and total fission) on the graphics screen.

plswrea - This subroutine is called to update plots for external and feedback reactivity versus time on the graphics screen.

plswpow - This subroutine is called to update power versus time plot on the graphics screen.

plreact - This subroutine is called to draw graph legends and titles for the reactivity versus time graphs.

plexper - This subroutine is called to plot the experimental data on the graphics screen.

plruler - This subroutine is called to plot the scaled ruler as an indicator for the solution height.

plinit - This subroutine initializes the plot windows.

sttpnt - This subroutine plots and updates the thermodynamic state (subcooled, superheated, or boiling) indicator on the graphics screen.

sfill - This subroutine is used to simulate the solution fill into the container on the graphics screen.

swith - This subroutine is used to simulate the transient rod withdrawal from the annular vessel on the graphics screen.

fcgeom - This function estimates the film cap geometry for the aerosol generation calculations.

aerogas - This subroutine conducts the aerosol generation calculations for the gas bubbles.

aerosteam - This subroutine conducts the aerosol generation calculations for the vapor bubbles.

inssus - This subroutine conducts the inherent neutron source strength calculations.

velx - This function returns the void bubble velocity.

kanjiwr - This subroutine is used to plot KANJI letters on the graphics screen.

The reader is referred to LSODE documentation for the detailed description of LSODE options and parameter.

Table A.2

Sample Input File for TRACE

$general	**title="CRAC16",amat="uni",amcn="sst" $end**
$lsode	**itol=1,rtol=1.d-5,atol=1.d-10,itask=1,istate=1,iopt=1,lrw=10090,liw=102,mf=10 $end**
$timing	**tend=7.6d2,tinc=1.d-3 $end**
$geometric	**nnradf=5,nnaxif=6 $end**
$neutronic	**irflg=4,ifflg=3,ieflg=5,amda=1.24d-2,3.05d-2,1.11d-1,3.01d-1,1.13d0,3.d0, beta=2.772d-4,1.761d-3,1.653d-3,3.168d-3,9.709d-4,3.120d-4,gen=3.76957E-05, sour=0.d0,bcoef=1.845896d-3,zext=2.2d-2,pd0=1.d-8,srp=12.d0,rhotmp1=-2.20304d-2, rhotmp2=-1.85218d-4,rhovoi1=-1.30918d2,rhovoi2=8.29402d2,rhovoi3=-1.12157d4, rhovoi4=5.76848d4,rhovoi5=-1.57243d5,rhovoi6=2.11341d5,rhovoi7=-1.15960d5, rhoext1=4.80881d1,rhoext2=-1.18989d2,rhoext3=1.05101d2,zlife=3.17872E-05, rhocon1=2.45802d-1,rhocon2=-4.08763d-3 $end**
$radgas	**ivgflg=3,icflg=1,vel1=1.2d-2,vdgsk=0.07d0,veldw=0.d0,velup=1.d0,gvalue=6.d-8, satc=-1.d0,a0=8.0d-8,a1=0.d0,a2=0.d0,b0=5.d-2,b1=0.d0,b2=3.d1,b4=0.d0,hmol=1.d1, rgbura=0.05d-6,ioflg=0 $end**
$thermal	**idflg=1,hitc=1.d-1,xy=2.95d2,tinf=2.95d2,ivar=6 $end**
$boiling	**iyflg=6,ikflg=1,ilflg=1,isflg=0,ivsflg=3,radeq=2.5d-6,cbc1=1.d-12,cbc2=3.d0, cbc3=0.d0,cbc4=0.d0,afreq=0.25d0,stbura=0.7d-6,svel1=1.2d-2,svdgsk=0.07d0, evcoef=5.d-3 $end**
$motion	**izflg=0,discof=2.6d3 $end**
$plot	**pdata="pow",ipflg=1,xmin=1.d14,xmax=1.d17,reamax=15.d0, reamin=-15.d0, voimax=24.d-3,voimin=0.d-3,tdelta=10.,tdelst=20.,iouti=100 $end**
$counter	**icrit=70 $end**
$pressure	**itflg=0,zcons=2.9d-5,pbias=6.9d4,prp=2.0d-3,gh2=1.1d0,prcons=2.d-8 $end**
$aero	**inflg=0,ihflg=1,iaflg=5,xperc=5.d1,fde=1.d0,fcth=0.d0,hdist1=1.d-1 $end**
$source	**ibflg=2 $end**

This is a blank page.

国際単位系（SI）と換算表

表1　SI基本単位および補助単位

量	名称	記号
長さ	メートル	m
質量	キログラム	kg
時間	秒	s
電流	アンペア	A
熱力学温度	ケルビン	K
物質量	モル	mol
光度	カンデラ	cd
平面角	ラジアン	rad
立体角	ステラジアン	sr

表2　SIと併用される単位

名称	記号
分，時，日	min，h，d
度，分，秒	°，′，″
リットル	l，L
トン	t
電子ボルト	eV
原子質量単位	u

1 eV=1.60218×10^{-19}J

1 u=1.66054×10^{-27}kg

表3　固有の名称をもつSI組立単位

量	名称	記号	他のSI単位による表現
周波数	ヘルツ	Hz	s^{-1}
力	ニュートン	N	m·kg/s^2
圧力，応力	パスカル	Pa	N/m^2
エネルギー，仕事，熱量	ジュール	J	N·m
工率，放射束	ワット	W	J/s
電気量，電荷	クーロン	C	A·s
電位，電圧，起電力	ボルト	V	W/A
静電容量	ファラド	F	C/V
電気抵抗	オーム	Ω	V/A
コンダクタンス	ジーメンス	S	A/V
磁束	ウェーバ	Wb	V·s
磁束密度	テスラ	T	Wb/m^2
インダクタンス	ヘンリー	H	Wb/A
セルシウス温度	セルシウス度	℃	
光束	ルーメン	lm	cd·sr
照度	ルクス	lx	lm/m^2
放射能	ベクレル	Bq	s^{-1}
吸収線量	グレイ	Gy	J/kg
線量等量	シーベルト	Sv	J/kg

表4　SIと共に暫定的に維持される単位

名称	記号
オングストローム	Å
バーン	b
バール	bar
ガル	Gal
キュリー	Ci
レントゲン	R
ラド	rad
レム	rem

1 Å=0.1nm=10^{-10}m

1 b=100fm^2=10^{-28}m^2

1 bar=0.1MPa=10^{5}Pa

1 Gal=1cm/s^2=10^{-2}m/s^2

1 Ci=3.7×10^{10}Bq

1 R=2.58×10^{-4}C/kg

1 rad=1cGy=10^{-2}Gy

1 rem=1cSv=10^{-2}Sv

表5　SI接頭語

倍数	接頭語	記号
10^{18}	エクサ	E
10^{15}	ペタ	P
10^{12}	テラ	T
10^{9}	ギガ	G
10^{6}	メガ	M
10^{3}	キロ	k
10^{2}	ヘクト	h
10^{1}	デカ	da
10^{-1}	デシ	d
10^{-2}	センチ	c
10^{-3}	ミリ	m
10^{-6}	マイクロ	μ
10^{-9}	ナノ	n
10^{-12}	ピコ	p
10^{-15}	フェムト	f
10^{-18}	アト	a

（注）

1．表1－5は「国際単位系」第5版，国際度量衡局1985年刊行による。ただし，1 eVおよび1 uの値はCODATAの1986年推奨値によった。

2．表4には海里，ノット，アール，ヘクタールも含まれているが日常の単位なのでここでは省略した。

3．barは，JISでは流体の圧力を表わす場合に限り表2のカテゴリーに分類されている。

4．EC閣僚理事会指令ではbar，barnおよび「血圧の単位」mmHgを表2のカテゴリーに入れている。

換算表

力	N(=10^{5}dyn)	kgf	lbf
	1	0.101972	0.224809
	9.80665	1	2.20462
	4.44822	0.453592	1

粘度　1 Pa·s(N·s/m^2)=10 P(ポアズ)(g/(cm·s))

動粘度　1m^2/s=10^{4}St(ストークス)(cm^2/s)

圧力	MPa(=10bar)	kgf/cm^2	atm	mmHg(Torr)	lbf/in^2(psi)
	1	10.1972	9.86923	7.50062×10^3	145.038
	0.0980665	1	0.967841	735.559	14.2233
	0.101325	1.03323	1	760	14.6959
	1.33322×10^{-4}	1.35951×10^{-3}	1.31579×10^{-3}	1	1.93368×10^{-2}
	6.89476×10^{-3}	7.03070×10^{-2}	6.80460×10^{-2}	51.7149	1

エネルギー・仕事・熱量	J(=10^7 erg)	kgf·m	kW·h	cal(計量法)	Btu	ft·lbf	eV
	1	0.101972	2.77778×10^{-7}	0.238889	9.47813×10^{-4}	0.737562	6.24150×10^{18}
	9.80665	1	2.72407×10^{-6}	2.34270	9.29487×10^{-3}	7.23301	6.12082×10^{19}
	3.6×10^6	3.67098×10^5	1	8.59999×10^5	3412.13	2.65522×10^6	2.24694×10^{25}
	4.18605	0.426858	1.16279×10^{-6}	1	3.96759×10^{-3}	3.08747	2.61272×10^{19}
	1055.06	107.586	2.93072×10^{-4}	252.042	1	778.172	6.58515×10^{21}
	1.35582	0.138255	3.76616×10^{-7}	0.323890	1.28506×10^{-3}	1	8.46233×10^{18}
	1.60218×10^{-19}	1.63377×10^{-20}	4.45050×10^{-26}	3.82743×10^{-20}	1.51857×10^{-22}	1.18171×10^{-19}	1

1 cal= 4.18605J（計量法）

= 4.184J（熱化学）

= 4.1855J（15℃）

= 4.1868J（国際蒸気表）

仕事率　1 PS(仏馬力)

= 75 kgf·m/s

= 735.499W

放射能	Bq	Ci
	1	2.70270×10^{-11}
	3.7×10^{10}	1

吸収線量	Gy	rad
	1	100
	0.01	1

照射線量	C/kg	R
	1	3876
	2.58×10^{-4}	1

線量当量	Sv	rem
	1	100
	0.01	1

（86年12月26日現在）

DEVELOPMENT OF A NEW SIMULATION CODE FOR EVALUATION OF CRITICALITY TRANSIENTS INVOLVING FISSILE SOLUTION BOILING